Ligand Stereoelectronic Effects in Complexes of Phospholanes, Phosphinanes, and Phosphepanes and Their Implications for Hydroformylation Catalysis

R. Angharad Baber, Mairi F. Haddow, Ann J. Middleton, A. Guy Orpen, and Paul G. Pringle*,†

School of Chemistry, University of Bristol, Cantocks Close, Bristol, U.K. BS8 1TS

Anthony Haynes* and Gary L. Williams

Department of Chemistry, University of Sheffield, Dainton Building, Brook Hill, Sheffield, U.K. S3 7HF

Rainer Papp

BASF Aktiengesellschaft, D-67056 Ludwigshafen, Germany

Received October 5, 2006

Convenient syntheses are described for the five-, six-, and seven-membered phosphacycles $PhP(CH_2)_{x-1}$, where $x = 5$ ($\mathbf{L^a_5}$), 6 ($\mathbf{L^a_6}$), 7 ($\mathbf{L^a_7}$), and $Bu^tP(CH_2)_{x-1}$ where $x = 5$ ($\mathbf{L^b_5}$), 6 ($\mathbf{L^b_6}$), 7 ($\mathbf{L^b_7}$). Treatment of $[PtCl_2(cod)]$ with $\mathbf{L^a_{5-7}}$ gives *cis*-$[PtCl_2(\mathbf{L^a_{5-7}})_2]$ ($\mathbf{1a_{5-7}}$), whereas with $\mathbf{L^b_{5-7}}$ a mixture of *cis*-$[PtCl_2(\mathbf{L^b_{5-7}})_2]$ ($\mathbf{1b_{5-7}}$) and *trans*-$[PtCl_2(\mathbf{L^b_{5-7}})_2]$ ($\mathbf{2b_{5-7}}$) is obtained. Metathesis of $\mathbf{1a_7}$ with NaI gives a mixture of *cis*-$[PtI_2(\mathbf{L^a_7})_2]$ ($\mathbf{3a_7}$) and *trans*-$[PtI_2(\mathbf{L^a_7})_2]$ ($\mathbf{4a_7}$). The crystal structures of $\mathbf{1a_5}$, $\mathbf{1a_6}$, $\mathbf{1a_7}$, and $\mathbf{4a_7}$ have been determined. Comparison of the structures of $\mathbf{1a_7}$ and $\mathbf{4a_7}$ reveals that $\mathbf{L^a_7}$ has variable steric bulk, with the crystallographically determined cone angle ranging from 137° (smaller than $\mathbf{L^a_5}$) to 172° (larger than $\mathbf{L^a_6}$), depending on the particular twist-chair seven-membered-ring conformations adopted. The complex *cis*-$[PtCl_2(\mathbf{L^b_6})]$ ($\mathbf{1b_6}$) is fluxional on the NMR time scale at ambient temperatures, as a result of restricted PtP rotation. Treatment of $[Rh_2Cl_2(CO)_4]$ with $\mathbf{L^a_{5-7}}$ or $\mathbf{L^b_{5-7}}$ gives the expected *trans*-$[RhCl(CO)(\mathbf{L^a_{5-7}})_2]$ ($\mathbf{5a_{5-7}}$) or *trans*-$[RhCl(CO)(\mathbf{L^b_{5-7}})_2]$ ($\mathbf{5b_{5-7}}$), and from the ν_{CO} values, it is deduced that the donor strengths to rhodium(I) are in the order $\mathbf{L^b_{5-7}} > \mathbf{L^a_{5-7}}$ and, within the $\mathbf{L^a}$ and $\mathbf{L^b}$ series, $\mathbf{L_7}$, $\mathbf{L_6} > \mathbf{L_5}$. An investigation into the kinetics of the oxidative addition of MeI to $\mathbf{5a_{5-7}}$ showed that the rate of reaction is in the order $\mathbf{5a_5} > \mathbf{5a_7} > \mathbf{5a_6}$; i.e., the smallest ligand gives the highest rate. It is postulated that the flexible $\mathbf{L^a_7}$ ligand adopts a lower bulk conformation and the order of decreasing rate is then in the order of increasing bulk. The rate of reaction of MeI with $\mathbf{5b_5}$ is 4 times faster than with $\mathbf{5a_5}$, but oxidative addition was not observed with $\mathbf{5b_6}$ or $\mathbf{5b_7}$, perhaps because steric congestion destabilizes the rhodium(III) product. A study of the rhodium-catalyzed hydroformylation of 1-octene is reported using ligands $\mathbf{L^a_{5-7}}$ and $\mathbf{L^b_{5-7}}$, but no systematic trends were observed, and the results for $\mathbf{L^a_{5-7}}$ were similar to those for the acyclic analogue $PhPEt_2$. An anomalous but reproducible result is that the catalyst derived from $\mathbf{L^b_7}$ shows negligible hydroformylation activity but rapid octene isomerization activity. The overall conclusion is that, with the rhodium complexes of the simple phosphacycles described here, no special effect of the rings was observed in the hydroformylation catalysis. An α-substituent effect is identified as a common feature in several high-activity hydroformylation catalysts derived from phosphinanes.

Introduction

The correlation of stereoelectronic effects in tertiary phosphine ligands with the reactivity of their coordination complexes is key to understanding their efficacy in homogeneous catalysis. Tolman's parameters (the cone angle, θ, and electronic parameter, ν_{CO}) remain the most widely used guides to the gross features of stereoelectronic effects for monodentate phosphorus(III) ligands.[1] However, subtle ligand structural effects can have significant consequences for the macroscopic properties of the complexes, as exemplified in this article, in which a comparative study of the ligand effects of two homologous series of cyclic phosphines is described.

The chemistry of phosphorus heterocycles is much less developed than the analogous nitrogen chemistry, and nowhere is this more true than in the area of coordination chemistry,[2] even though cyclic phosphines have been shown to be excellent ligands for catalysis and particularly hydroformylation catalysis.[3−6]

* To whom correspondence should be addressed.

† E-mail: paul.pringle@bristol.ac.uk. Fax: +44 (0)117 929 0509. Tel: +44 (0)117 928 8114.

(1) (a) Tolman, C. A. *Chem. Rev.* **1977**, *77*, 313. (b) Bunten, K. A.; Chen, L.; Fernandez, A. L.; Poë, A. J. *Coord. Chem. Rev.* **2002**, *233−234*, 41 and references therein.

(2) (a) Mathey, F. In *Phosphorus-Carbon Heterocyclic Chemistry*; Pergamon Press: Oxford, U.K., 2001. (b) Doherty, R.; Haddow, M. F.; Harrison, Z. A.; Orpen, A. G.; Pringle, P. G.; Turner, A.; Wingad, R. L. *Dalton Trans.* **2006**, 4310 and references therein.

(3) (a) Mason, R. F.; van Winkle, J. L. U.S. Patent 3 400 163, 1968 (to Shell); (b) Steynberg J. P.; Govender, K.; Steynberg, P. J. World Patent WO 14248, 2002 (to Sasol).

10.1021/om060912v CCC: $37.00
Publication on Web 12/29/2006

In this article, the complexes of the two series of phosphacycles $\mathbf{L^a}_{5-7}$ and $\mathbf{L^b}_{5-7}$ with platinum(II) and rhodium(I) are reported

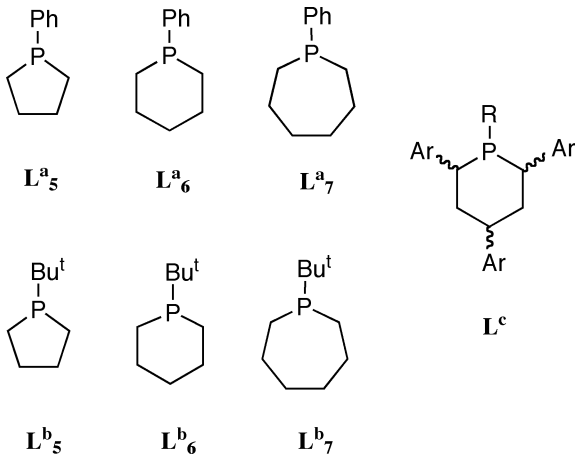

and their spectroscopic and crystallographic properties are used to probe their σ-/π-bonding characteristics. The rates of oxidative addition of MeI to rhodium(I) complexes of $\mathbf{L^a}_{5-7}$ and $\mathbf{L^b}_{5-7}$ have been measured, and the results are interpreted in terms of ligand stereoelectronic effects. Finally, the hydroformylation of 1-octene catalyzed by rhodium complexes of $\mathbf{L^a}_{5-7}$ and $\mathbf{L^b}_{5-7}$ has been investigated, in the hope that these studies would shed light on the remarkably high hydroformylation activity of rhodium complexes of $\mathbf{L^c}$ reported by BASF.[4]

Results and Discussion

Ligand Synthesis. The phosphacycles $\mathbf{L^a_{5,6}}$ were first synthesized over 90 years ago[7] by the reaction of the corresponding $BrMgCH_2(CH_2)_nCH_2MgBr$ ($n = 2, 3$) with $PhPCl_2$, and more recently[8] all three $\mathbf{L^a}_{5-7}$ compounds have been made by intramolecular ring closure reactions of $PhP(H)(CH_2)_nCH{=}CH_2$ ($n = 2-4$). The NMR spectroscopic properties of $\mathbf{L^a}_{5-7}$ have been extensively discussed,[9] but their coordination chemistry has been little studied.[10,11,12] The *tert*-butylphosphacycles $\mathbf{L^b_{5,6}}$ have been previously made by substitution reactions of Bu^t-PCl_2[13] or Bu^{t}P(OMe)$_2$,[14] but the seven-membered 1-*tert*-butylphosphepane ($\mathbf{L^b_7}$) is new. Rhodium complexes of $\mathbf{L^b_{5,6}}$ have been shown to catalyze the production of ethylene glycol from CO/H_2 mixtures.[15] We prepared all the phenylphosphacycles $\mathbf{L^a}_{5-7}$ and *tert*-butylphosphacycles $\mathbf{L^b}_{5-7}$ by the route shown in eq 1, which is an extension of Jolly's synthesis[14] of

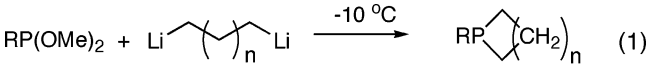

(1)

$\mathbf{L^a_{5-7}}$ n = 2 - 4, R = Ph

$\mathbf{L^b_{5-7}}$ n = 2 - 4, R = Bu^t

1-*tert*-butylphospholane ($\mathbf{L^b_5}$). An improvement to the procedure was that the dilithiated alkanes were generated in situ by scaling up Negishi's method[16] (eq 2). These one-pot syntheses are

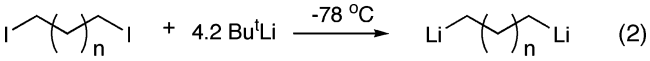

(2)

n = 2 - 4

convenient, and pure products are readily obtained, but the yields are at best modest.

Platinum(II) Complexes. Addition of 2 equiv of each of the phosphacycles $\mathbf{L^a}_{5-7}$ and $\mathbf{L^b}_{5-7}$ to $[PtCl_2(cod)]$ afforded the complexes $[PtCl_2(L)_2]$ ($\mathbf{1a}_{5-7}$, $\mathbf{1b}_{5-7}$, $\mathbf{2b}_{5-7}$) as air-stable solids. These complexes were characterized by a combination of ^{31}P, ^1H, and ^{13}C NMR spectroscopy, mass spectrometry, elemental analysis, and X-ray crystallography. The geometries of the complexes were ascertained from the ^1J(PtP) coupling constants (see Table 1) and in some cases were confirmed by crystal structure determinations (see below). The geometry depended on the P substituent; the phenylphosphacycles $\mathbf{L^a}_{5-7}$ gave cis complexes $\mathbf{1a}_{5-7}$, whereas the more bulky ligands $\mathbf{L^b}_{5-7}$ gave a mixture of cis complexes $\mathbf{1b}_{5-7}$ and trans complexes $\mathbf{2b}_{5-7}$ (eq 3). From the data given in Table 1, the five-membered

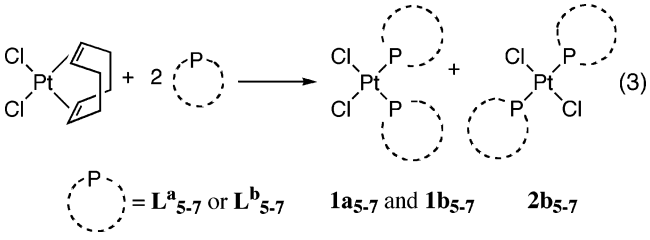

(3)

P = $\mathbf{L^a}_{5-7}$ or $\mathbf{L^b}_{5-7}$ $\mathbf{1a}_{5-7}$ and $\mathbf{1b}_{5-7}$ $\mathbf{2b}_{5-7}$

phosphacycles have consistently the highest δ_P and $\Delta\delta$ values and the lowest ^1J(PtP) values, which may be associated with the hybridization required at P to accommodate the smaller C−P−C angles (see further discussion below).

Table 1. $^{31}P\{^1H\}$ NMR Data for the Complexes $[PtCl_2(L)_2]^a$

ligand	complex	δ/ppm	J(PtP)/Hz	$\Delta\delta$
$\mathbf{L^a_5}$	$\mathbf{1a_5}$	14.7	3524	30.0
$\mathbf{L^a_6}$	$\mathbf{1a_6}$	−10.9	3533	23.7
$\mathbf{L^a_7}$	$\mathbf{1a_7}$	3.1	3559	29.2
$\mathbf{L^b_5}$	$\mathbf{1b_5}$	35.7[b]	3481	33.6
$\mathbf{L^b_5}$	$\mathbf{2b_5}$	40.5[b]	2386	38.4
$\mathbf{L^b_6}$	$\mathbf{1b_6}$	10.6[b]	3601	23.2
$\mathbf{L^b_6}$	$\mathbf{2b_6}$	16.6	2433	29.2
$\mathbf{L^b_7}$	$\mathbf{1b_7}$	22.3[b]	3591	29.2
$\mathbf{L^b_7}$	$\mathbf{2b_7}$	22.9[b]	2407	29.8
$\mathbf{L^a_7}$	$\mathbf{3a_7}$	2.0	3400	28.1
$\mathbf{L^a_7}$	$\mathbf{4a_7}$	−3.8	2307	22.8

[a] Spectra measured in $CDCl_3$ unless stated otherwise. [b] Spectrum measured in CD_2Cl_2.

(4) Mackewitz, T.; Ahlers, W.; Zeller, E.; Röper, M.; Paciello, R.; Knoll, K.; Papp, R. World Patent WO 00669, 2002 (to BASF).
(5) Breit, B.; Fuchs, E. *Chem. Commun*. **2004**, 694.
(6) Baber, R. A.; Clarke, M. L.; Heslop, K.; Marr, A. C.; Orpen, A. G.; Pringle, P. G.; Ward, A.; Zambrano-Williams, D. E. *Dalton Trans.* **2005**, 1079.
(7) (a) Gruttner, G.; Wiernik, M. *Chem. Ber*. **1915**, *48*, 1473. (b) Gruttner, G.; Krause, E. *Chem. Ber*. **1916**, *49*, 437.
(8) Davies, J. H.; Downer, J. D.; Kirby, P. *J. Chem. Soc. C* **1966**, 245.
(9) (a) Gray, G. A.; Cramer, S. E.; Marsi, K. L. *J. Am. Chem. Soc.* **1976**, *98*, 2109. (b) Chestnut, D. B.; Quin, L. D.; Wild, S. B. *Heteroat. Chem.* **1997**, *8*, 451.
(10) (a) Coles, S. J.; Edwards, P. G.; Hursthouse, M. B.; Abdul Malik, K. M.; Thick, J. L.; Tooze, R. P. *J. Chem. Soc., Dalton Trans.* **1997**, 1821. (b) Bader, A.; Kang, Y. B.; Pabel, M.; Pathak, D. D.; Willis, A. C.; Wild, S. B. *Organometallics* **1995**, *14*, 1434.
(11) Bodner, G. M.; May, M. P.; McKinney, L. E. *Inorg. Chem.* **1980**, *19*, 1951.
(12) Shima, T.; Bauer, E. B.; Hampel, F.; Gladysz, J. A. *Dalton Trans*. **2004**, 1012.
(13) Featherman, S. I.; Lee, S. O.; Quin, L. D. *J. Org. Chem.* **1974**, *39*, 2899.
(14) Emrich, R.; Jolly, P. W. *Synthesis* **1993**, 39.
(15) (a) Yoshida, S.; Ogomori, Y; Watanabe, Y.; Honda, K.; Goto, M.; Kurahashi, M. *J. Chem. Soc., Dalton Trans.* **1988**, 895. (b) Ogomori, Y; Yoshida, S.; Watanabe, Y. *J. Mol. Catal*. **1987**, *43*, 249.
(16) Negishi, E.; Swanson, D. R.; Rousset, C. J. *J. Org. Chem.* **1990**, *55*, 5406.

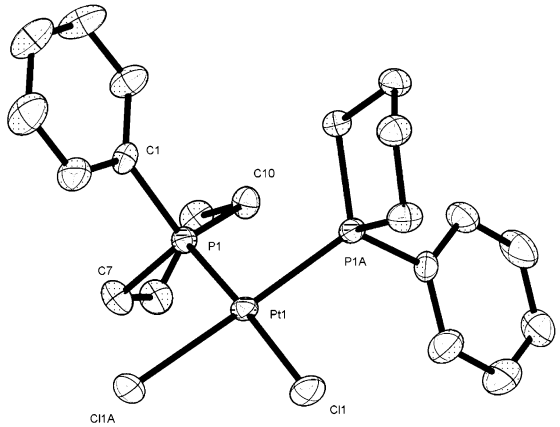

Figure 1. ORTEP plot of **1a$_5$**. All hydrogen atoms have been omitted for clarity.

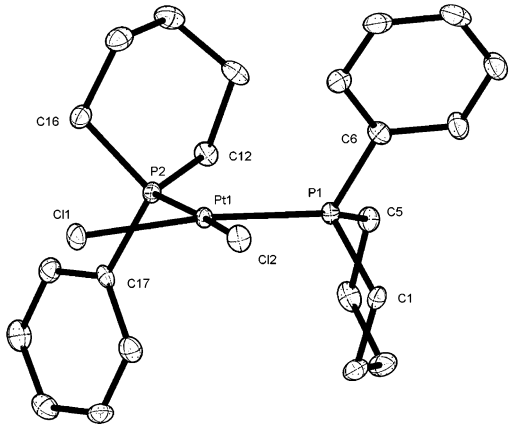

Figure 2. ORTEP plot of **1a$_6$**. All hydrogen atoms have been omitted for clarity.

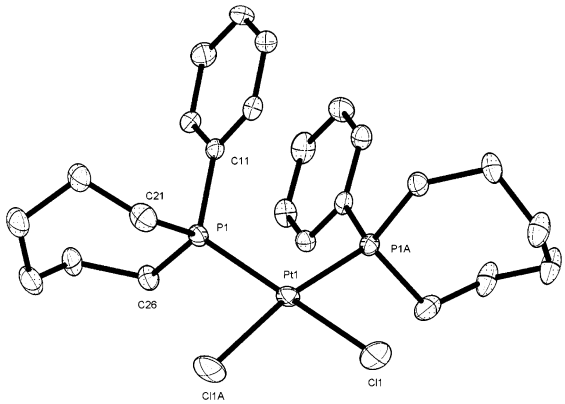

Figure 3. ORTEP plot of **1a$_7$**. All hydrogen atoms have been omitted for clarity.

Single crystals of **1a$_{5-7}$** were grown by various methods (see the Experimental Section) and their structures determined by X-ray crystallography (see Figures 1−3 and Tables 2−4). The phenyl substituents in **1a$_{5,6}$** are anti with respect to each other, and the six-membered rings in **1a$_6$** adopt chair conformations with the phenyl groups in equatorial positions.

There is an intramolecular offset parallel $\pi-\pi$ interaction[17] between the phenyl substituents in **1a$_7$** with a close distance between the C_6H_5 rings of 3.145 Å (C11−C11′).[18] In order to investigate the conformations of ligand **L$^a_7$** in the absence of the $\pi-\pi$ interactions present in complex **1a$_7$**, the diiodoplatinum analogue was made, in anticipation that the bulky iodo ligands would promote a trans geometry. In fact, treatment of **1a$_7$** with NaI gave a mixture of *cis*- and *trans*-[PtI$_2$(**L$^a_7$**)$_2$] (**3a$_7$** and **4a$_7$**) (see the Experimental Section and Table 1 for the data) but the trans isomer **4a$_7$** readily crystallized and its structure was determined (see Figure 4 and Table 5).

Table 2. Selected Bond Lengths (Å) and Angles (deg) for *cis*-[PtCl$_2$(L$^a_5$)$_2$] (1a$_5$)

Pt1−P1	2.2397(9)	P1−C10	1.837(3)
Pt1−Cl1	2.3686(10)	P1−C7	1.850(3)
P1−C1	1.823(3)		
C1−P1−C10	108.87(16)	C10−P1−C7	94.42(16)
C1−P1−C7	106.05(16)	P1−Pt1−P1−C7	148.67(14)

Table 3. Selected Bond Lengths (Å) and Angles (deg) for *cis*-[PtCl$_2$(L$^a_6$)$_2$] (1a$_6$)

Pt1−P2	2.2479(9)	P1−C1	1.824(4)
Pt1−P1	2.2541(9)	P1−C6	1.826(4)
Pt1−Cl1	2.3566(9)	P2−C12	1.818(4)
Pt1−Cl2	2.3595(9)	P2−C17	1.825(4)
P1−C5	1.820(4)	P2−C16	1.827(4)
C5−P1−C1	97.69(18)	Cl2−Pt1−P1−C6	−65.17(13)
C5−P1−C6	105.87(18)	P1−Pt1−P2−C17	110.10(12)
C1−P1−C6	104.90(17)		

Table 4. Selected Bond Lengths (Å) and Angles (deg) for *cis*-[PtCl$_2$(L$^a_7$)$_2$] (1a$_7$)

Pt1−P1	2.2454(11)	P1−C26	1.833(4)
Pt1−Cl1	2.3631(12)	P1−C21	1.837(5)
P1−C11	1.825(4)		
C11−P1−C26	108.3(2)	C26−P1−C21	109.0(2)
C11−P1−C21	99.2(2)	P1A−Pt1−P1−C11	−26.23(15)

A comparison of selected bond length and angles and ligand cone angles for the platinum complexes [PtX$_2$(**L$^a_{5-7}$**)$_2$] can be made from the data collected in Table 6. Inspection of the intracyclic C−P−C angles reveals that this angle is compressed by reduction in the size of the phosphacycle, as expected. There is a considerable difference between the intracyclic C−P−C angles of **1a$_7$** and **4a$_7$**, and this variation is presumably a consequence of the flexibility of the seven-membered ring.

Seven-membered rings adopt four low-energy conformations,[19] and calculations on their relative energies have shown[20] that the twist chair is the minimum energy form. Indeed, the seven-membered rings in **1a$_7$** and **4a$_7$** both adopt twist-chair conformations but the position of the phosphorus atom within the twist chair gives the ligand quite different steric demands, which can be seen more clearly by viewing the Pt−ligand fragments in **1a$_7$** and **4a$_7$**, as shown in Figure 5. The conformation adopted by **L$^a_7$** in **4a$_7$** gives it much greater steric demands than the **L$^a_7$** in **1a$_7$** and this is reflected in the calculated cone angles (Table 6). Notably, the cone angle for **L$^a_7$** in **4a$_7$** is significantly larger than that for **L$^a_6$** in **1a$_6$** and the cone angle for **L$^a_7$** in **1a$_7$** is smaller than that for **L$^a_5$** in **1a$_5$**. A further

(17) Hunter, C. A.; Sanders, J. K. M. *J. Am. Chem. Soc.* **1990**, *112*, 5525.

(18) Janiak, J. *Dalton Trans*. **2000**, 3885.

(19) (a) Testa, B. In *Principles of Organic Stereochemistry*; Marcel Dekker: New York, 1979. (b) Anet, F. A. L. In *Conformational Analysis of Medium-Sized Heterocycles*; Glass, R. S., Ed.; VCH: New York, 1988.

(20) Favini, G. *J. Mol. Struct.* **1983**, *93*, 139.

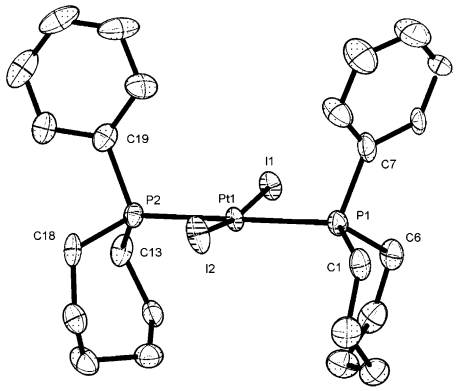

Figure 4. ORTEP plot of **4a$_7$**. All hydrogen atoms have been omitted for clarity.

Table 5. Selected Bond Lengths (Å) and Angles (deg) for *trans*-[PtI$_2$(L$^a_7$)$_2$] (4a$_7$)

Pt1−P1	2.3229(19)	P1−C1	1.829(8)
Pt1−P2	2.3225(19)	P1−C7	1.818(9)
Pt1−I2	2.6140(6)	P2−C18	1.817(8)
Pt1−I1	2.6201(6)	P2−C13	1.832(8)
P1−C6	1.816(8)	P2−C19	1.820(9)
C6−P1−C1	101.4(4)	C1−P1−C7	100.4(4)
C6−P1−C7	105.2(4)		

Table 6. Selected Bond Lengths (Å) and Angles (deg) for Complexes [PtX$_2$(L$^a_{5-7}$)$_2$] (X = Cl, I)

	1a$_5$	**1a$_6$**	**1a$_7$**	**4a$_7$**
Pt−P	2.239(1)	2.253(1)	2.246(1)	2.3229(19)
Pt−X	2.367(1)	2.359(1)	2.363(1)	2.6140(6)
C−P−C (cyclic)	94.6(2)	97.5(2)	109.0(2)	101.4(4)
P−Pt−P	92.60(6)	103.11(4)	99.67(6)	176.54(7)
X−Pt−X	88.30(7)	87.32(4)	88.29(7)	171.20(2)
cone angle	140	164, 161	137	160, 173

complication in assessing the bulk of the phenylphosphacycles is that the value of the cone angle (given by eq 4) is highly

$$\theta = \frac{2}{3}\sum \alpha + \frac{180}{\pi}\sin^{-1}\left(\frac{r_H}{d}\right) \qquad (4)$$

$$\alpha = \text{P−M−H angle}, d = \text{M−H}$$

dependent on the orientation of the phenyl ring; i.e., the closer the torsion angle Pt−P−C−C is to 90°, the smaller the contribution the phenyl group makes to the cone angle (as shown by angle α in Figure 6). The orientation of the phenyl ring affects the value of α by up to 30°, which thereby affects the cone angle by up to 20°, all other atoms being consistent. For complexes **1a$_{5-7}$**, **4a$_7$**, and **5a$_5$** (see below), the torsions of the phenyl rings are 132, 0/159, 131, 0/57, and 100°, respectively.

The ^{31}P NMR spectra (see Table 1) of the products of the reactions of [PtCl$_2$(cod)] with the bulky ligands **L$^b_{5-7}$** in CH_2Cl_2 showed that both cis and trans isomers were formed, which is consistent with the bulk of **L$^b_{5-7}$** being greater than that of **L$^a_{5-7}$**. When the reactions were carried out in toluene, the cis isomers **1b$_{5-7}$** precipitated from the reaction mixture, while the trans isomers **2b** remained in solution. There was no evidence of cis/trans isomerization when either isomer was redissolved in CD_2Cl_2 for periods of weeks.

Crystals of **1b$_6$** and **2b$_6$** were grown by slow diffusion of Et_2O into their saturated CH_2Cl_2 solutions and their crystal structures determined (see Figures 7 and 8 and Tables 7 and 8). A comparison of selected bond lengths and angles and cone

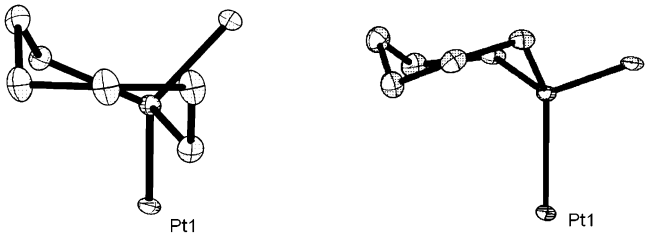

1a$_7$ **4a$_7$**

Figure 5. Pt−ligand fragments of the crystal structures, showing the seven-membered-ring conformations.

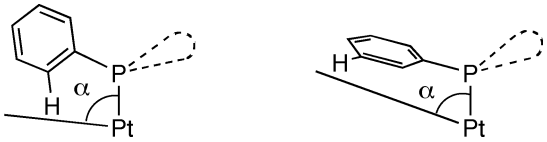

Figure 6. Effect of orientation of the phenyl substituent on the size of α, which contributes to the cone angle.

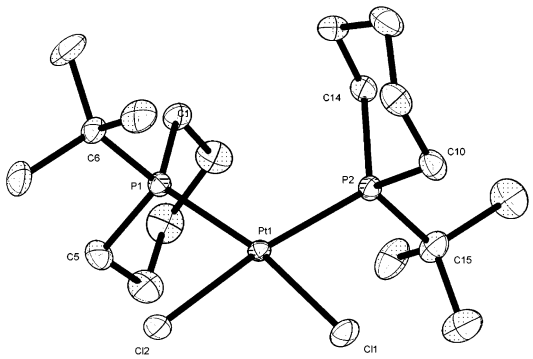

Figure 7. ORTEP plot of **1b$_6$**. All hydrogen atoms have been omitted for clarity.

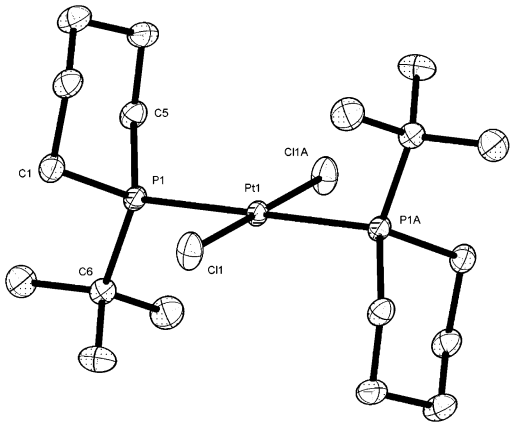

Figure 8. ORTEP plot of **2b$_6$**. All hydrogen atoms have been omitted for clarity.

angles for the platinum complexes *cis*- and *trans*-[PtCl$_2$(**L$^b_6$**)$_2$] can be made from the data in Table 9. Both structures show **L$^b_6$** in a chair conformation with the *tert*-butyl substituents in pseudoequatorial positions, and there is little difference in the intracyclic C−P−C angles or the calculated cone angles for **L$^b_6$**.

The room-temperature ^{31}P{^{1}H} NMR spectrum of **1b$_6$** showed a broad singlet with platinum satellites. Cooling the solution to −40 °C revealed the presence of two species in the ratio ca. 50:1, and the ^1J(PtP) values showed that, in both species, the phosphines are cis to each other (Figure 9). The free energy barrier to the process was estimated from the coalescence

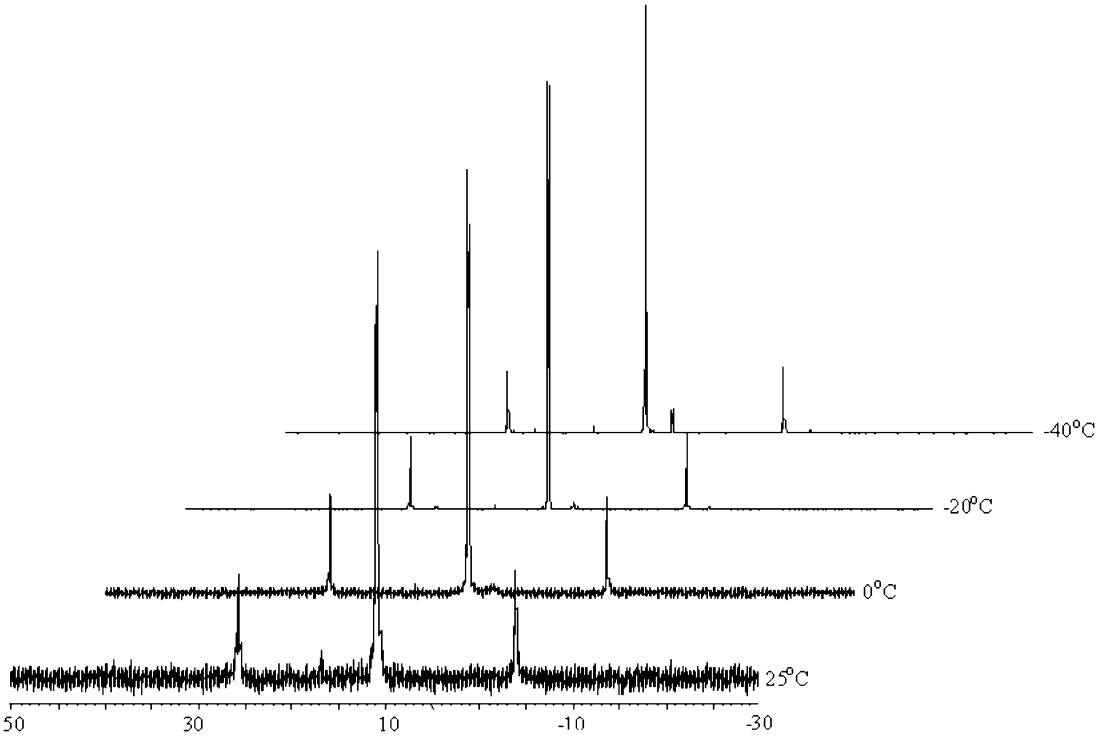

Figure 9. Variable-temperature ^{31}P NMR of **1b$_6$**.

Table 7. Selected Bond Lengths (Å) and Angles (deg) for *cis*-[PtCl$_2$(L$^b_6$)$_2$] (1b$_6$)

Pt1−P2	2.2656(15)	P1−C5	1.828(6)
Pt1−P1	2.2754(15)	P1−C6	1.889(6)
Pt1−Cl1	2.3573(15)	P2−C14	1.824(6)
Pt1−Cl2	2.3629(15)	P2−C10	1.836(6)
P1−C1	1.817(6)	P2−C15	1.897(7)
C1−P1−C5	97.0(3)	C14−P2−C15	105.9(3)
C1−P1−C6	106.5(3)	C10−P2−C15	106.0(3)
C5−P1−C6	108.2(3)	P2−Pt1−P1−C6	−114.4(2)
C14−P2−C10	98.0(3)	P1−Pt1−P2−C15	−109.8(2)

Table 8. Selected Bond Lengths (Å) and Angles (deg) for *cis*-[PtCl$_2$(L$^b_6$)$_2$] (2b$_6$)

Pt1−Cl1	2.3161(6)	P1−C1	1.824(2)
Pt1−P1	2.3185(5)	P1−C6	1.858(2)
P1−C5	1.824(2)		
C5−P1−C1	99.46(11)	C1−P1−C6	106.98(10)
C5−P1−C6	108.48(10)		

Table 9. Selected Bond Lengths (Å) and Angles (deg) for Complexes *cis*- and *trans*-[PtCl$_2$(L$^b_6$)$_2$]

	1b$_6$	**2b$_6$**
Pt−P	2.2754(15)	2.3185(5)
Pt−Cl	2.3629(15)	2.3161(6)
C−P−C (cyclic)	97.0(3)	99.46(11)
P−Pt−P	104.12(5)	180
Cl−Pt−Cl	84.77(6)	180
cone angle	165, 158	163

temperature[21] (T_c 283 K) to be 52 (±1) kJ mol^{-1}. We tentatively suggest that these two isomers are rotamers and the fluxionality is due to restricted rotation about the Pt−P bonds. Barriers to M−P rotation in complexes containing *trans*-M(PR$_3$)$_2$ moieties have been measured[22] to be in the range 36−75 kJ mol^{-1}, but to the best of our knowledge, barriers to rotation in complexes containing a *cis*-M(PR$_3$)$_2$ moiety have not been previously reported. The crystal structure of **1b$_6$** shows that the exocyclic P substituents are anti to each other and there is pseudo (though not crystallographic) C_2 symmetry; this is represented schematically in Figure 10a. Another possible rotamer (which is presumably more crowded and therefore less stable) is one where the substituents are syn to each other and the structure has C_s symmetry (depicted in Figure 10b). The fluxionality in solution may be due to the interconversion of these C_2 and C_s isomers.

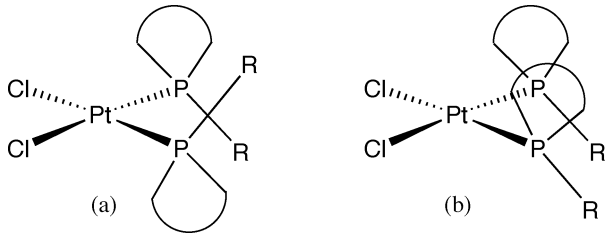

Figure 10. Suggested rotomers present in solution with (a) C_2 symmetry and (b) C_s symmetry.

Rhodium(I) Complexes. Addition of 4 equiv of phosphacycles **L$^a_{5-7}$** and **L$^b_{5-7}$** to [Rh$_2$Cl$_2$(CO)$_4$] in hexane afforded the complexes *trans*-[RhCl(CO)(L)$_2$] as yellow solids which precipitated from solution (eq 5). These complexes were

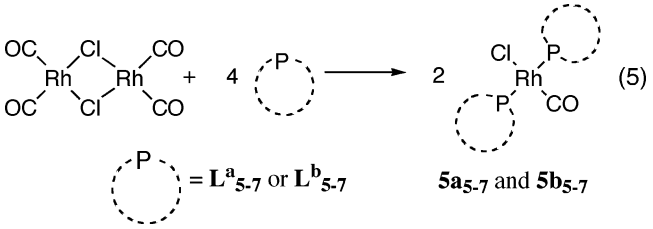

(21) Sandström, J. In *Dynamic NMR Spectroscopy*; Academic Press: London, 1982; p 96.

(22) (a) Baber, R. A.; Orpen, A. G.; Pringle, P. G.; Wilkinson, M. J.; Wingad, R. L. *Dalton Trans.* **2005**, 659 and references therein. (b) Bushweller, C. H.; Hoogasian, S.; English, A. D.; Miller, J. S.; Lourandos, M. Z. *Inorg. Chem.* **1981**, *20*, 3448. (c) Dwyer, C. L.; Kirk, M. M.; Meyer, W. H.; van Rensburg, W. J.; Forman, G. S. *Organometallics* **2006**, *25*, 3806.

characterized by a combination of ^{31}P, ^{1}H, and ^{13}C NMR spectroscopy, mass spectrometry, elemental analysis, IR spectroscopy, and X-ray crystallography. The ^{31}P NMR spectra for all the rhodium complexes showed a doublet, consistent with a trans geometry, and these data, together with the CO stretching frequencies for the complexes, are collected in Table 10. The values of ν(CO) indicate[23] that the *tert*-butylphosphacycles are stronger σ-donors than their phenylphosphacycle analogues. In addition, the data are consistent with the five-membered rings being weaker σ-donors/stronger π-acceptors than the six- and seven-membered analogues, a conclusion that is also supported by the ^{1}J(PtP) values given in Table 1 and is in agreement with the prediction from the Walsh diagram of a lower energy HOMO and lower energy LUMO as the C−P−C angle is compressed.[24]

Table 10. ^{31}P NMR[a] and IR Data[b] for the Complexes [RhCl(CO)(L)$_2$]

ligand	complex	δ/ppm	J(RhP)/Hz	ν(CO)/cm^{-1}
$\mathbf{L^a_5}$	$\mathbf{5a_5}$	28.2	118	1968
$\mathbf{L^a_6}$	$\mathbf{5a_6}$	6.4	117	1960
$\mathbf{L^a_7}$	$\mathbf{5a_7}$	18.1	118	1962
$\mathbf{L^b_5}$	$\mathbf{5b_5}$	49.0[c]	117	1955
$\mathbf{L^b_6}$	$\mathbf{5b_6}$	27.8[c]	118	1950
$\mathbf{L^b_7}$	$\mathbf{5b_7}$	34.8[c]	118	1951

[a] Spectra measured in $CDCl_3$ unless otherwise stated. [b] Spectra measured in CH_2Cl_2. [c] In CD_2Cl_2.

Single crystals of $\mathbf{5a_5}$ and $\mathbf{5b_{5-7}}$ were grown by various methods (see the Experimental Section) and the crystal structures determined (see Figures 11−14 and Tables 11−14).

A comparison of selected bond lengths and angles and cone angles for the rhodium complexes [RhCl(CO)(**L**)$_2$] can be made from the data given in Table 15. The intracyclic C−P−C angles show the expected trend, with the smaller rings having smaller angles at phosphorus. The cone angles for the *tert*-butylphosphines are larger than those for the corresponding phenylphosphines of the same ring size. In this series of rhodium complexes there is a monotonic trend with the larger rings having a larger cone angle.

With the exception of $\mathbf{4a_7}$ and $\mathbf{5a_5}$, the trans complexes of Pt(II) and Rh(I) reported here have crystallographic inversion symmetry (or pseudo inversion symmetry for the Rh(I) complexes, where the chlorine and carbonyl ligands are disordered). None of the complexes adopt C_s symmetry, although it would certainly be plausible sterically and the C_2 conformation adopted by $\mathbf{5a_5}$ is very close to C_{2v} symmetry. Also, with the exception of $\mathbf{5a_5}$, all the complexes adopt a conformation such that the torsion angles Cl−Pt−P−R (where R is the exocyclic substituent on the phosphine) are close to 90°. The torsion angles R−P−P−R are close to (or exactly) 180°, except for $\mathbf{4a_7}$, where R−P−P−R is close to 0°.

Oxidative Addition of Methyl Iodide to the Rhodium(I) Complexes. The spectroscopic and crystallographic data for the platinum(II) and rhodium(I) complexes of $\mathbf{L^a_{5-7}}$ and $\mathbf{L^b_{5-7}}$ discussed above lead to the following generalizations about the stereoelectronic properties of the phosphacyclic ligands.

(a) The *tert*-butylphosphacycles $\mathbf{L^b_{5-7}}$ are stronger donors than the analogous phenylphosphacycles $\mathbf{L^a_{5-7}}$.

(b) The five-membered phospholanes are weaker donors than the analogous six-membered phosphinanes or seven-membered phosphepanes (which are similar in their donor properties).

(23) Vastag, S.; Heil, B.; Markó, L. *J. Mol. Catal.* **1979**, *5*, 189.

(24) (a) Orpen, A. G.; Connelly, N. G. *Chem. Commun.* **1985**, 1310. (b) Orpen, A. G.; Connelly, N. G. *Organometallics* **1990**, *9*, 1206.

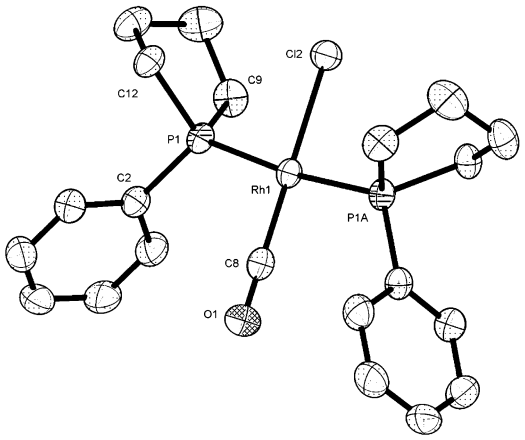

Figure 11. ORTEP plot of $\mathbf{5a_5}$. All hydrogen atoms have been omitted for clarity.

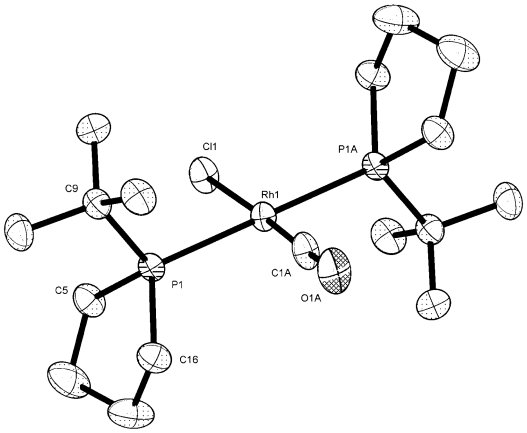

Figure 12. ORTEP plot of $\mathbf{5b_5}$. All hydrogen atoms and the image of the disordered CO and Cl ligands have been omitted for clarity.

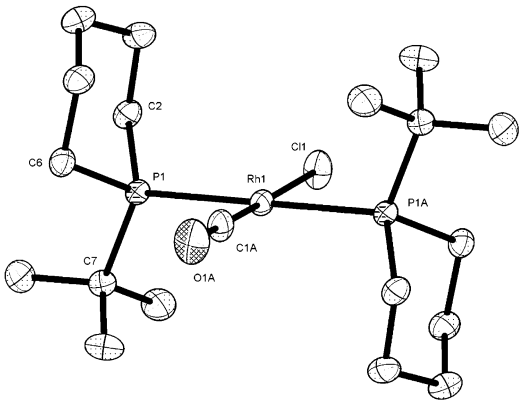

Figure 13. ORTEP plot of $\mathbf{5b_6}$. All hydrogen atoms and the image of the disordered CO and Cl ligands have been omitted for clarity.

Table 11. Selected Bond Lengths (Å) and Angles (deg) for *trans*-[RhCl(CO)(L$^a_5$)$_2$] ($\mathbf{5a_5}$)

Rh1−C8	1.819(4)	P1−C2	1.824(2)
Rh1−P1	2.3133(6)	P1−C12	1.839(2)
Rh1−Cl2	2.3675(10)	P1−C9	1.852(2)
C2−P1−C12	104.44(11)	C12−P1−C9	93.82(11)
C2−P1−C9	103.65(11)		

(c) The phospholanes are smaller than the phosphinanes, but phosphepanes are flexible and so allow conformations that can be larger than the chair conformation of the six-membered phosphacycle or smaller than the envelope conformation of phospholanes.

Table 12. Selected Bond Lengths (Å) and Angles (deg) for *trans*-[RhCl(CO)(L^a_5)$_2$] ($5b_5$)

Rh1−C1	1.734(8)	P1−C16	1.850(3)
Rh1−P1	2.3311(6)	P1−C5	1.855(3)
Rh1−Cl1	2.414(3)	P1−C9	1.861(3)
C16−P1−C5	93.77(13)	C5−P1−C9	107.54(12)
C16−P1−C9	106.86(13)		

Table 13. Selected Bond Lengths (Å) and Angles (deg) for *trans*-[RhCl(CO)(L^a_5)$_2$] ($5b_6$)

Rh1−C1	1.729(5)	P1−C2	1.8301(18)
Rh1−P1	2.3333(5)	P1−C6	1.8332(17)
Rh1−Cl1	2.429(2)	P1−C7	1.8621(19)
C2−P1−C6	99.08(8)	C6−P1−C7	106.27(8)
C2−P1−C7	107.80(8)		

Table 14. Selected Bond Lengths (Å) and Angles (deg) for *trans*-[RhCl(CO)(L^a_5)$_2$] ($5b_7$)

Rh1−C11	1.757(8)	P1−C6	1.830(2)
Rh1−P1	2.3207(7)	P1−C1	1.837(2)
Rh1−Cl1	2.388(3)	P1−C7	1.872(2)
C6−P1−C1	101.27(12)	C1−P1−C7	103.90(11)
C6−P1−C7	104.39(12)		

Table 15. Selected Bond Lengths (Å) and Angles (deg) for Complexes [RhCl(CO)(L)$_2$]

	$5a_5$	$5b_5$	$5b_6$	$5b_7$
Rh−P	2.3133(5)	2.3311(6)	2.3335(6)	2.3207(7)
Rh−C	1.816(3)	1.734(8)	1.721(7)	1.757(8)
C−O	1.143(4)	1.169(8)	1.168(7)	1.167(11)
Rh−Cl	2.3673(9)	2.414(3)	2.428(3)	2.388(3)
C−P−C (cyclic)	93.58(11)	93.77(13)	99.22(10)	101.27(12)
P−Rh−P	173.17(3)	180	180	180
C−Rh−Cl	180	177.2(2)	178.97(18)	177.5(4)
cone angle	124	146	161	172

The oxidative addition of MeI to the complexes *trans*-[RhCl(CO)($\mathbf{L^a_{5-7}}$)$_2$] and *trans*-[RhCl(CO)($\mathbf{L^b_{5-7}}$)$_2$] was studied in detail to explore whether the reactivity trends could be interpreted in terms of these ligand stereoelectronic effects. Previous investigations[25] have shown that the kinetics of MeI oxidative addition to square-planar Rh(I) complexes (and the tendency for migratory CO insertion to occur in the Rh(III)−methyl product) are very sensitive to the nature of the coligands.

The reactions of MeI with $\mathbf{5a_{5-7}}$ and $\mathbf{5b_{5-7}}$ were monitored by IR spectroscopy under pseudo-first-order conditions (excess MeI). Reactions were observed at relatively low [MeI] (0.08−0.32 mol dm^{-3}) for the three phenyl phosphacycle complexes, $\mathbf{5a_{5-7}}$, the ν(CO) band of the Rh(I) reactant being replaced in each case by an absorption at higher frequency (Table 16), consistent with the oxidative addition product [RhCl(I)(Me)(CO)(L)$_2$]. The products recovered after the kinetic runs were also analyzed by NMR spectroscopy, and the data are given in Table 16. The ^{1}H NMR spectra showed triplets of doublets due to coupling of the methyl protons to ^{103}Rh and to two equivalent ^{31}P nuclei. As well as the principal methyl resonance for each product, some weaker triplets of doublets were also observed, indicating the presence of additional Rh methyl complexes. Similarly, the ^{31}P NMR spectra exhibited up to four doublets with Rh−P coupling. The NMR data can be explained by scrambling of halide ligands in the product to give a mixture containing [RhCl$_2$(Me)(CO)(L)$_2$] and [RhI$_2$(Me)(CO)(L)$_2$] as well as isomers of [RhCl(I)(Me)(CO)(L)$_2$] with methyl trans to Cl or I (eq 6).

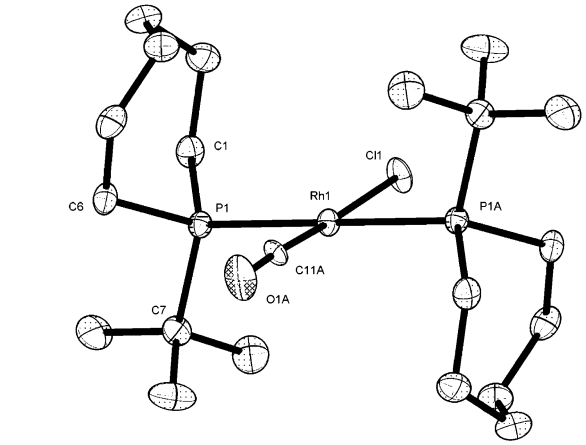

Figure 14. ORTEP plot of $\mathbf{5b_7}$. All hydrogen atoms and the image of the disordered CO and Cl ligands have been omitted for clarity.

Table 16. IR[a] and NMR[b] Spectroscopic Data for Products [RhX$_2$(Me)(CO)(L)$_2$] (X = Cl, I) Arising from Oxidative Addition of MeI to $5a_{5-7}$ and $5b_{5-7}$

L	ν(CO)/ cm^{-1}	δ(^{1}H)/ppm (Rh−CH_3)[c]	δ(^{31}P)/ppm (^1J(RhP)/Hz)
$\mathbf{L^a_5}$	2059	1.05, 0.72 (8:1)	33.4 (85), 28.5 (85), 19.3 (76), 27.9 (74)
$\mathbf{L^a_6}$	2050	0.59, 0.45, 0.80 (5.5:1:0.4)	14.5 (82), 17.6 (82),4.1 (72), 10.8 (71)
$\mathbf{L^a_7}$	2055	0.75, 0.47 (vw), 0.83 (vw)	4.0 (84), 8.7 (83), −6.5 (74), −4.4 (84)
$\mathbf{L^b_5}$	2036	1.23, 0.95 (vw)	57.6 (84), 62.7 (83)
$\mathbf{L^b_6}$	2030		
$\mathbf{L^b_7}$	2029		

[a] Spectra measured in CH_2Cl_2. [b] Spectra measured in $CDCl_3$. [c] All triplets of doublets with ^2J(RhH) and ^3J(PH) ca. 2 and 5 Hz, respectively.

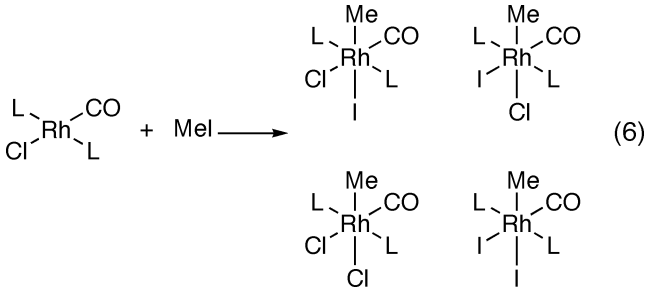

Despite the mixtures of products indicated by NMR spectroscopy, plots of IR absorbance versus time for the Rh(I) reactants were very well fitted by exponential decays, showing that the reactions are first order with respect to the Rh(I) complex. Pseudo-first-order rate constants (k_{obs}) were measured as a function of [MeI] and temperature and are reported in the Supporting Information. Plots of k_{obs} vs [MeI] were linear, indicating a first-order dependence on the alkyl halide and therefore a second-order reaction overall. Values of the second-order rate constants obtained from the slopes of these plots are given in Table 17. Eyring plots of the variable-temperature data also showed good linearity and yielded the activation parameters listed in Table 17. These are similar in magnitude for $\mathbf{5a_{5-7}}$, and the large negative $\Delta S^{\ddagger}$ values are typical of MeI oxidative

(25) (a) Gonsalvi, L.; Adams, H.; Sunley, G. J.; Ditzel, E.; Haynes, A. *J. Am. Chem. Soc.* **1999**, *121*, 11233. (b) Gonsalvi, L.; Adams, H.; Sunley, G. J.; Ditzel, E.; Haynes, A. *J. Am. Chem. Soc.* **2002**, *124*, 13597. (c) Gonsalvi, L.; Gaunt, J. A.; Adams, H.; Castro, A.; Sunley, G. J.; Haynes, A. *Organometallics* **2003**, *22*, 1047. (d) Martin, H. C.; James, N. H.; Aitken, J.; Gaunt, J. A.; Adams, H.; Haynes, A. *Organometallics* **2003**, *22*, 4451.

Table 17. Second-Order Rate Constants (k_1, 25 °C, CH_2Cl_2) and Activation Parameters for Oxidative Addition of MeI to $\mathbf{5a_{5-7}}$ and $\mathbf{5b_{5-7}}$

reactant	$10^3\ k_1$/dm^3 mol^{-1} s^{-1}	$\Delta H^{\ddagger}$/kJ mol^{-1}	$\Delta S^{\ddagger}$/J K^{-1} mol^{-1}
$\mathbf{5a_5}$	11.6	45 ± 3	-132 ± 9
$\mathbf{5a_6}$	2.83	43 ± 1	-149 ± 2
$\mathbf{5a_7}$	8.59	41 ± 1	-147 ± 2
$\mathbf{5b_5}$	42.8	37 ± 2	-147 ± 7
$\mathbf{5b_6}$	small		
$\mathbf{5b_7}$	0.015[a]		

[a] Calculated from kinetics for approach to equilibrium and estimated equilibrium constant.

addition proceeding via an S_N2 mechanism.[26] The observed order of reactivity for the phenyl phosphacycle complexes is $\mathbf{5a_5} > \mathbf{5a_7} > \mathbf{5a_6}$ (k_{rel} ca. 4:3:1), which appears to be determined predominantly by ligand steric properties. Thus, the complex of the smallest phosphacycle gives the highest rate, despite this being the least electron rich (on the basis of ν(CO) values). The higher reactivity of $\mathbf{5a_7}$ compared to that of $\mathbf{5a_6}$ can be explained if the flexible phosphepane $\mathbf{L^a_7}$ adopts a conformation of lower bulk than the phosphinane $\mathbf{L^a_6}$, thereby accommodating the crowding in the S_N2 transition state.

A more dramatic effect of ligand steric bulk on reactivity was found for the *tert*-butyl phosphacycle complexes, $\mathbf{5b_{5-7}}$. The least hindered complex of this series, $\mathbf{5b_5}$, reacted with MeI in a manner similar to that described above for $\mathbf{5a_{5-7}}$. NMR spectroscopy again indicated a mixture of Rh(III) methyl products resulting from halide scrambling in [RhCl(I)(Me)(CO)-($\mathbf{L^b_5}$)$_2$] (Table 16). Kinetic measurements showed that $\mathbf{5b_5}$ is more reactive than all the phenyl phosphacycle complexes, its second-order rate constant for MeI addition (Table 17) being nearly 4 times larger than that for $\mathbf{5a_5}$. This rate enhancement, which arises largely from a lowering of $\Delta H^{\ddagger}$, is attributed to an electronic effect, the stronger donor $\mathbf{L^b_5}$ making the rhodium complex more nucleophilic. It is notable that complexes $\mathbf{5a_{5-7}}$ and $\mathbf{5b_5}$ are more reactive toward MeI (by factors of 2−30) than *trans*-[RhI(CO)(PEt$_3$)$_2$] (ν(CO) 1961 cm^{-1}; $k_1 = 1.37 \times 10^{-3}$ dm^3 mol^{-1} s^{-1}), studied by Cole-Hamilton and coworkers.[27]

In contrast to the relatively high reactivity of $\mathbf{5b_5}$, the two most sterically congested complexes, $\mathbf{5b_6}$ and $\mathbf{5b_7}$, did not give stable oxidative addition products when treated with MeI. Only at high MeI concentrations was evidence found for formation of Rh(III) methyl products. When $\mathbf{5b_7}$ was dissolved in neat MeI, IR spectroscopy indicated initial attainment of an equilibrium between the reactant and a species with ν(CO) at 2029 cm^{-1}, assigned as [RhCl(I)(Me)(CO)($\mathbf{L^b_7}$)$_2$]. At equilibrium (attained after ca. 1 h at 25 °C) approximately 25% of $\mathbf{5b_7}$ was converted into product, corresponding to an equilibrium constant of ca. 0.02 dm^3 mol^{-1} for the oxidative addition reaction. The approach to equilibrium followed first-order kinetics with a rate constant of 1×10^{-3} s^{-1}, which will contain contributions from both forward and reverse rates ($k_{obs} = k_1$[MeI] + k_{-1}). This leads to estimates of $k_1 = 1.5 \times 10^{-5}$ dm^3 mol^{-1} s^{-1} and $k_{-1} = 7.6 \times 10^{-4}$ s^{-1}. Thus, the oxidative addition rate constant for $\mathbf{5b_7}$ is ca. 3000 times smaller than that for $\mathbf{5b_5}$. When it was monitored for longer time periods, the ν(CO) band due to $\mathbf{5b_7}$ shifted slightly (1−2 cm^{-1}) to higher frequency, indicating halide exchange with MeI to give the iodide analogue, [RhI-(CO)($\mathbf{L^b_7}$)$_2$]. This shift was accompanied by a decrease in ν-(CO) band intensity for the MeI addition product, indicating that the equilibrium constant for oxidative addition to [RhI-(CO)($\mathbf{L^b_7}$)$_2$] is smaller than for the chloride, $\mathbf{5b_7}$. Oxidative addition of MeI was found to be even less favorable for $\mathbf{5b_6}$. In neat MeI, a weak IR band appeared at 2030 cm^{-1}, consistent with formation of a small amount of [RhCl(I)(Me)(CO)($\mathbf{L^b_6}$)$_2$]. On the basis of the IR intensities, only about 4% of $\mathbf{5b_6}$ is converted to the product in neat MeI, suggesting that the equilibrium constant for oxidative addition is an order of magnitude smaller for $\mathbf{5b_6}$ than for $\mathbf{5b_7}$. Over extended time periods, the ν(CO) band for $\mathbf{5b_6}$ shifted ca. 2 cm^{-1} to higher frequency, consistent with halide exchange, giving [RhI(CO)-($\mathbf{L^b_6}$)$_2$].

The dramatically lower reactivity of $\mathbf{5b_{6,7}}$ compared with that of $\mathbf{5b_5}$ and $\mathbf{5a_{5-7}}$ is an example of the operation of a steric threshold.[28] Severe steric congestion by ligands $\mathbf{L^b_6}$ and $\mathbf{L^b_7}$ hinders the oxidative addition of methyl iodide and makes the six-coordinate rhodium(III) products thermodynamically unstable. Interestingly, no evidence was found in these systems for migratory CO insertion. In principle, conversion of an octahedral methyl carbonyl complex into a square-pyramidal acetyl complex can provide an alternative route by which steric congestion can be relieved, as observed in a number of related systems. Methyl migration to CO in the products arising from MeI addition to $\mathbf{5b_{6,7}}$ is probably inhibited by the relatively electron rich metal center, which imparts considerable back-donation to the CO ligand. In other Rh(III) systems where steric promotion of methyl migration has been observed, ν(CO) values were typically 30−50 cm^{-1} higher than for [RhCl(I)(Me)(CO)-($\mathbf{L^b_{6,7}}$)$_2$].[25] The instability conferred by steric congestion in the latter is therefore relieved by reductive elimination of MeI rather than by methyl migration.

The main conclusions from the kinetics are as follows.

(a) The rates of oxidative addition of MeI to the complexes *trans*-[RhCl(CO)($\mathbf{L^a_{5-7}}$)$_2$] ($\mathbf{5a_{5-7}}$) are in the order $\mathbf{5a_5} > \mathbf{5a_7} > \mathbf{5a_6}$, which correlates better with the steric properties of the ligands than with the electronic properties. That is, the complex of the smallest phosphacycle gives the highest rate and it is postulated that the flexible phosphepane $\mathbf{L^a_7}$ adopts a conformation of lower bulk than the phosphinane $\mathbf{L^a_6}$ to accommodate the crowding in the rhodium(III) product.

(b) The *tert*-butylphospholane complex *trans*-[RhCl(CO)-($\mathbf{L^b_5}$)$_2$] ($\mathbf{5b_5}$) undergoes oxidative addition of MeI 4 times faster than *trans*-[RhCl(CO)($\mathbf{L^a_5}$)$_2$], consistent with the stronger donor $\mathbf{L^b_5}$ making the rhodium complex more nucleophilic.

(c) In contrast to $\mathbf{5b_5}$, only when neat MeI was used was evidence obtained for very slow oxidative addition of MeI to the complexes of the more bulky phosphacycles *trans*-[RhCl-(CO)($\mathbf{L^b_6}$)$_2$] ($\mathbf{5b_6}$) and *trans*-[RhCl(CO)($\mathbf{L^b_7}$)$_2$] ($\mathbf{5b_7}$). It is likely that this is a consequence of steric congestion destabilizing the rhodium(III) product; once again the evidence suggests that the seven-membered phosphacycle ($\mathbf{L^b_7}$) behaves as if it were smaller than the six-membered analogue ($\mathbf{L^b_6}$).

Hydroformylation Catalysis. The ligands $\mathbf{L^a_{5-7}}$ and $\mathbf{L^b_{5-7}}$ were tested for the rhodium-catalyzed hydroformylation of 1-octene, and the results are shown in Table 18. For the phenyl phosphacycles $\mathbf{L^a_{5-7}}$ (entries 1−3) and the noncyclic analogue PPhEt$_2$ (entry 4), essentially the same *n*-aldehyde selectivity is obtained. In terms of activity $\mathbf{L^a_5}$ and $\mathbf{L^a_6}$ showed lower activity than $\mathbf{L^a_7}$, which had activity similar to that of PPhEt$_2$; it would

(26) (a) Griffin, T. R.; Cook, D. B.; Haynes, A.; Pearson, J. M.; Monti, D.; Morris, G. E. *J. Am. Chem. Soc.* **1996**, *118*, 3029. (b) Rendina, L. M.; Puddephatt, R. J. *Chem. Rev.* **1997**, *97*, 1735. (c) Labinger, J. A.; Osborn, J. A. *Inorg. Chem.* **1980**, *19*, 3230.

(27) (a) Rankin, J.; Poole, A. D.; Benyei, A. C.; Cole-Hamilton, D. J. *Chem. Commun*. **1997**, 1835. (b) Rankin, J.; Benyei, A. C.; Poole, A. D.; Cole-Hamilton, D. J. *J. Chem. Soc., Dalton Trans*. **1999**, 3771.

(28) Eriks, K.; Giering, W. P.; Liu, H. Y.; Prock, A. *Inorg. Chem*. **1989**, *28*, 1759.

Table 18. Hydroformylation of 1-Octene[a]

entry	ligand	all C_8 olefins/ mol %	nonanals/ mol %	*n*-selectivity/ %
1	$\mathbf{L^a_5}$	0.9	26.3	66.5
2	$\mathbf{L^a_6}$	0.6	19.5	67.7
3	$\mathbf{L^a_7}$	1.8	88.0	67.0
4	$PPhEt_2$	1.8	88.0	67.0
5	$\mathbf{L^b_5}$	2.7	88.0	62.0
6	$\mathbf{L^b_6}$	3.7	88.0	54.0
7	$\mathbf{L^b_7}$	82.8	4.7	4.3
8	PPh_3	1.2	89.7	67.8

[a] Products obtained after 4 h reaction in toluene/1-octene at 90 °C and 10 bar of H_2/CO with [Rh] = 5 μM, 10/1 ratio of L to Rh, and ca. 7000/1 ratio of 1-octene to Rh. See the Experimental Section for full details.

appear that constraining the P donor in a ring reduces the activity of the catalyst for this series.

The results for the *tert*-butyl phosphacycles $\mathbf{L^b_{5-7}}$ (entries 5−7) show that the *tert*-butyl group leads to more active catalysts for the five- and six-membered phosphacycles (compare entries 5 and 6 with entries 1 and 2). The anomalous result with $\mathbf{L^b_7}$ (entry 7) showing negligible hydroformylation activity but rapid olefin isomerization activity was reproducible with different batches of ligands. This may be another manifestation of a threshold effect in which apparently very small differences in ligand structure produce a sharply different catalytic profile.

The hydroformylation study has not detected any systematic trends in catalyst performance related to the structure of the phosphacycles $\mathbf{L^a_{5-7}}$ and $\mathbf{L^b_{5-7}}$. This leads us to conclude that the source of the extraordinarily high efficiency of the BASF catalyst[4] derived from $\mathbf{L^c}$ is more likely to be the position and bulk of the substituents on the α-carbons rather than a stereoelectronic effect associated with the C−P−C angle in the phosphinane ring. The α-substituent effect could be a more general phenomenon; for example, the high activity of the rhodium hydroformylation catalysts derived from cyclic phosphines[5,6] $\mathbf{L^d}$ and $\mathbf{L^e}$ may also be a consequence of the ligands having bulky α-substituents.

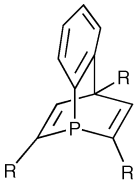

$\mathbf{L^d}$

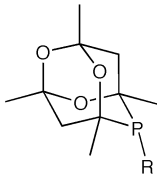

$\mathbf{L^e}$

Experimental Section

General Procedures. Unless otherwise stated, all reactions were carried out under a dry nitrogen atmosphere using standard Schlenk line techniques. Dry N_2-saturated solvents were collected from a Grubbs solvent system[29] in flame- and vacuum-dried glassware. MeOH was dried over 3 Å molecular sieves and deoxygenated by N_2 saturation. Commercial reagents were used as supplied unless otherwise stated. All phosphines were stored under nitrogen at room temperature. Most complexes were stable to air in the solid state and were stored in air at room temperature. The starting materials $[PtCl_2(cod)]$[30] and $[RhCl(CO)_2]_2$[31] were prepared by literature methods. Elemental analyses were carried out by The Microanalytical Laboratory of the School of Chemistry, University of Bristol. Electron impact and fast atom bombardment mass spectra were recorded by The Mass Spectrometry Service, University of Bristol, on MD800 and Autospec instruments. Infrared spectroscopy was carried out on a Perkin-Elmer 1600 Series FTIR spectrometer. NMR spectra were measured on a JEOL GX 300, JEOL Eclipse 400, or JEOL GX 400 spectrometer. $^{31}P\{^1H\}$, $^{13}C\{^1H\}$, and ^1H NMR spectra were recorded at ambient temperature of the probe at 300, 100, and 121 MHz, respectively, using deuterated solvent to provide the field/frequency lock.

Synthesis of 1-Phenylphospholane ($\mathbf{L^a_5}$). To a solution of t-BuLi (100 cm^3, 1.7 M in pentane, 0.17 mol) in Et_2O (50 cm^3) was added 1,4-diiodobutane (5.34 cm^3, 12.544 g, 0.041 mol) over 5 min at −78 °C. The reaction mixture was stirred at −78 °C for 100 min, before being warmed to room temperature and added dropwise to a solution of phenyldimethoxyphosphine (6.20 cm^3, 0.036 mol) in hexane (150 cm^3) at −10 °C. The resultant solution was stirred at −15 °C for 5 h, washed with water (3 × 50 cm^3), and dried over $MgSO_4$. The solution was filtered and the solvent removed under reduced pressure to leave a yellow oil, which was distilled under reduced pressure (ca. 0.1 mmHg, bp 57−59 °C) using a 20 cm^3 Vigreux column to give $\mathbf{L^a_5}$ as a colorless liquid (3.0 cm^3, 3.50 g, 59% yield). ^{31}P NMR ($CDCl_3$): δ_P −15.3 (s).

Synthesis of 1-Phenylphosphinane ($\mathbf{L^a_6}$). To a solution of t-BuLi (200 cm^3, 1.7 M in pentane, 0.34 mol) in Et_2O (100 cm^3) was added 1,5-diiodopentane (6.02 cm^3, 26.22 g, 0.081 mol) over 30 min at −78 °C. The reaction mixture was stirred at −78 °C for 16 h, before being warmed to room temperature and added dropwise to a solution of phenyldimethoxyphosphine (11.65 cm^3, 0.072 mol) in hexane (250 cm^3) at −10 °C. The resultant solution was stirred at −15 °C for 5 h, washed with water (3 × 100 cm^3), and dried over $MgSO_4$. The solution was filtered and the solvent removed under reduced pressure to leave a yellow oil, which was distilled under reduced pressure (ca. 0.1 mmHg, bp 50−54 °C) using a 20 cm^3 Vigreux column to give $\mathbf{L^a_6}$ as a colorless liquid (2.5 cm^3, 2.58 g, 19% yield). ^{31}P NMR ($CDCl_3$): δ_P −34.3 (s).

Synthesis of 1-Phenylphosphepane ($\mathbf{L^a_7}$). To a solution of t-BuLi (200 cm^3, 1.7 M in pentane, 0.34 mol) in Et_2O (100 cm^3) was added 1,6-diiodohexane (11.4 cm^3, 24.8 g, 0.146 mol) over 10 min at −78 °C. The reaction mixture was stirred at −78 °C for 16 h, before being warmed to room temperature and added dropwise to a solution of phenyldimethoxyphosphine (11.4 cm^3, 12.4 g, 0.073 mol) in hexane (250 cm^3) at −10 °C. The resultant solution was stirred at −15 °C for 3 h, washed with water (3 × 100 cm^3), and dried over $MgSO_4$. The solution was filtered and the solvent removed under reduced pressure to leave a yellow oil, which was distilled under reduced pressure (ca. 0.1 mmHg, bp 63−73 °C) using a 20 cm^3 Vigreux column to give $\mathbf{L^a_7}$ as a colorless liquid (0.8 cm^3, 0.824 g, 6% yield). ^{31}P NMR ($CDCl_3$): δ_P −26.1 (s).

Synthesis of 1-*tert*-Butylphospholane ($\mathbf{L^b_5}$). To a solution of t-BuLi (183 cm^3, 1.5 M in pentane, 0.275 mol) in Et_2O (100 cm^3) was added 1,4-diiodobutane (8.74 cm^3, 20.1 g, 0.065 mol) over 15 min at −78 °C. The reaction mixture was stirred at −78 °C for 4 h, before being warmed to room temperature overnight. To a solution of trimethyl phosphite (6.9 cm^3, 7.3 g, 0.059 mol) in hexane (200 cm^3) was added t-BuLi (39.2 cm^3, 1.5 M in pentane, 0.059 mol) dropwise over 15 min at −78 °C, and then the mixture was warmed to room temperature overnight. A solution of 1,4-dilithiobutane was added dropwise to a solution of *tert*-butyldimethoxyphosphine at −10 °C over 1 h. The resultant solution was stirred at −10 °C for 2 h and at room temperature for 4 days and then washed with water (3 × 100 cm^3) and dried over $MgSO_4$. The solution was filtered and the solvent removed under reduced pressure to leave a yellow oil, which was distilled under reduced pressure (53 mmHg, bp 76−80 °C) using a 10 cm^3 Vigreux column to give $\mathbf{L^b_5}$ as a colorless liquid (1.702 g, 20% yield). Anal. Found (calcd): C, 66.48 (66.64); H, 12.41 (11.88). ^{31}P NMR ($CDCl_3$): δ_P 2.1 (s). ^1H NMR ($CDCl_3$): δ_H 1.75−1.56 (m, 6H), 1.54−1.42 (m, 2H), 0.96 (d, CH_3, 9H, $^3J(PH)$ = 11.7 Hz). ^{13}C NMR ($CDCl_3$):

(29) Pangborn, A. B.; Giardello, M. A.; Grubbs, R. H.; Rosen, R. K.; Timmers, F. J. *Organometallics* **1996**, *15*, 1518.
(30) McDermott, J. X.; White, J. F.; Whitesides, G. M. *J. Am. Chem. Soc.* **1976**, *98*, 6521.
(31) McCleverty, J. A.; Wilkinson, G. *Inorg. Synth.* **1990**, *28*, 212.

δ_C 28.5 (d, CH_2CH_2P, ^2J(PC) = 1.5 Hz), 27.4 (d, CH_3, ^2J(PC) = 13.8 Hz), 21.9 (d, CH_2P, ^1J(PC) = 15.4 Hz), tertiary carbon not seen.

Synthesis of 1-*tert*-Butylphosphinane (L^b_6). To a solution of t-BuLi (200 cm^3, 1.7 M in pentane, 0.34 mol) in Et_2O (100 cm^3) was added 1,5-diiodopentane (12.05 cm^3, 26.2 g, 0.081 mol) over 15 min at −78 °C. The reaction mixture was stirred at −78 °C for 4 h, before being warmed to room temperature overnight. To a solution of trimethyl phosphite (8.6 cm^3, 9.0 g, 0.073 mol) in hexane (200 cm^3) was added t-BuLi (42.7 cm^3, 1.7 M in pentane, 0.073 mol) dropwise over 15 min at −78 °C, and then the mixture was warmed to room temperature overnight. A solution of 1,5-dilithiopentane was added dropwise to a solution of *tert*-butyldimethoxyphosphine at 5 °C over 30 min. The resultant solution was stirred at room temperature for 72 h and then washed with water (3 × 100 cm^3) and dried over $MgSO_4$. The solution was filtered and the solvent removed under reduced pressure to leave a yellow oil, which was distilled under reduced pressure (20 mmHg, bp 62−66 °C) using a 10 cm^3 Vigreux column to give $\mathbf{L^b_6}$ as a colorless liquid (4 cm^3, 3.9 g, 38% yield). Satisfactory elemental analyses for this compound were not obtained despite clean NMR spectra, presumably because of its extreme air sensitivity. Anal. Found (calcd): C, 66.68 (68.32); H, 12.57 (12.10). ^{31}P NMR ($CDCl_3$): δ_P −12.6 (s). ^{1}H NMR ($CDCl_3$): δ_H 2.05−1.90 (m, 2H), 1.72−1.63 (m, 1H), 1.62−1.43 (m, 4H), 1.32−1.00 (m, 3H), 0.97 (d, 9H, C*H*$_3$, ^3J(PH) = 11.5 Hz). ^{13}C NMR ($CDCl_3$): δ_C 28.2 (d, *C*H$_2$, *J*(PC) = 3.1 Hz), 26.8 (d, *C*H$_3$, ^2J(PC) = 13.1 Hz), 24.9 (d, *C*H$_2$, *J*(PC) = 5.4 Hz), 20.8 (d, *C*H$_2$P, ^1J(PC) = 14.6 Hz), tertiary carbon not seen.

Synthesis of 1-*tert*-Butylphosphepane (L^b_7). To a solution of t-BuLi (200 cm^3, 1.7 M in pentane, 0.34 mol) in Et_2O (100 cm^3) was added 1,6-diiodohexane (13.53 cm^3, 27.4 g, 0.081 mol) over 15 min at −78 °C. The reaction mixture was stirred at −78 °C for 4 h, before being warmed to room temperature overnight. To a solution of trimethyl phosphite (8.6 cm^3, 9.0 g, 0.073 mol) in hexane (200 cm^3) was added t-BuLi (42.7 cm^3, 1.7 M in pentane, 0.073 mol) dropwise over 15 min at −78 °C, and then the mixture was warmed to room temperature overnight. The solution of 1,6-dilithiohexane was added dropwise to the solution of *tert*-butyldimethoxyphosphine at room temperature over 1 h. The resultant solution was stirred at room temperature for 48 h and then at 50 °C for 48 h before being washed with water (3 × 100 cm^3) and then dried over $MgSO_4$. The solution was filtered and the solvent removed under reduced pressure to leave a yellow oil, which was distilled under reduced pressure (20 mmHg, bp 82−88 °C) using a 10 cm^3 Vigreux column to give $\mathbf{L^b_7}$ as a colorless liquid (2.6 cm^3, 2.6 g, 21% yield). Satisfactory elemental analyses for this compound were not obtained despite clean NMR spectra, presumably because of its extreme air sensitivity. Anal. Found (calcd): C, 68.83 (69.73); H, 12.25 (12.29). ^{31}P NMR ($CDCl_3$): δ_P −6.9 (s). ^{1}H NMR ($CDCl_3$): δ_H 2.00−1.77 (m, 2H), 1.75−1.53 (m, 6H), 1.53−1.30 (m, 4H), 0.98 (d, C*H*$_3$, 9H, C*H*$_3$, ^3J(PH) = 11.2 Hz). ^{13}C NMR ($CDCl_3$): δ_C 27.9 (d, *C*H$_2$, *J*(PC) = 4.6 Hz), 27.1 (d, *C*H$_3$, ^2J(PC) = 13.1 Hz), 26.1 (d, *C*H$_2$, *J*(PC) = 10.0 Hz), 23.9 (d, *C*H$_2$P, ^1J(PC) = 16.9 Hz), tertiary carbon not seen.

Preparation of *cis*-[$PtCl_2(L^a_5)_2$] ($\mathbf{1a_5}$). To a suspension of [$PtCl_2$(cod)] (0.130 g, 0.35 mmol) in toluene (3 cm^3) was added a solution of $\mathbf{L^a_5}$ (0.114 g, 0.69 mmol) in toluene (2 cm^3). The resulting light yellow solution was stirred for 12 h. The solvent was removed under reduced pressure to leave a cream-colored solid, which was recrystallized from CH_2Cl_2/Et_2O to give a fine white powder (0.105 g, 0.18 mmol, 51% yield). X-ray-quality crystals were grown from a saturated methanol solution. Anal. Found (calcd): C, 40.44 (40.42); H, 4.68 (4.41). ^{31}P NMR ($CDCl_3$): δ_P 14.7 (s, *J*(PtP) = 3524 Hz). ^{1}H NMR ($CDCl_3$): δ_H 7.3−7.8 (m, 5H, Ar *H*), 2.4−2.7 (m, 2H), 2.1−2.2 (m, 2H), 1.6−2.0 (m, 4H). ^{13}C NMR ($CDCl_3$): δ_C 131.7 (m), 131.4 (m), 131.0 (s, Ar *C*), 128.6 (m), 28.1 (m, *C*H$_2$), 26.5 (s, *C*H$_2$ *J*(PtC) = 25 Hz). FAB mass spectrum: *m*/*z* 594 (M$^+$), 559 (M$^+$ − Cl).

Preparation of *cis*-[$PtCl_2(L^a_6)_2$] ($\mathbf{1a_6}$). To a solution of $\mathbf{L^a_6}$ (0.204 g, 1.14 mmol) in CH_2Cl_2 (2 cm^3) was added [$PtCl_2$(cod)] (0.214 g, 0.572 mmol). After the reaction mixture was stirred for 12 h, the solvent was reduced to ca. 1 cm^3 and Et_2O (40 cm^3) was added. The resulting white precipitate was filtered off, washed with Et_2O, and dried under reduced pressure to afford the desired product as a white powder (0.260 g, 0.41 mmol, 73% yield). X-ray-quality crystals were grown by slow diffusion of Et_2O into a saturated CH_2Cl_2 solution. Anal. Found (calcd): C, 42.49 (42.45); H, 4.88 (4.86). ^{31}P NMR ($CDCl_3$): δ_P −10.9 (s, *J*(PtP) = 3533 Hz). ^{1}H NMR ($CDCl_3$): δ_H 7.6−7.7 (m, 2H, Ar *H*), 7.4−7.5 (m, 3H, Ar *H*), 2.5−2.7 (m, 2H), 1.8−2.0 (m, 2H), 1.6−1.8 (m, 2H), 1.2−1.6 (m, 4H). ^{13}C NMR ($CDCl_3$): δ_C 131.4 (t, Ar *C*, *J*(PC) = 5 Hz), 130.9 (s, Ar *C*), 129.8 (m, Ar *C*), 128.7 (t, Ar *C*, *J*(PC) = 5 Hz), 26.1 (s, C*H*$_2$), 24.4 (m, *C*H$_2$), 22.3 (s, *C*H$_2$). FAB mass spectrum: *m*/*z* 622 (M$^+$), 587 (M$^+$ − Cl).

Preparation of *cis*-[$PtCl_2(L^a_7)_2$] ($\mathbf{1a_7}$). To a solution of $\mathbf{L^a_7}$ (0.179 g, 0.93 mmol) in CH_2Cl_2 (2 cm^3) was added [$PtCl_2$(cod)] (0.174 g, 0.47 mmol). After the reaction mixture was stirred for 12 h, the solvent was reduced to ca. 1 cm^3 and Et_2O (40 cm^3) was added. The resulting white precipitate was filtered off, washed with Et_2O, and dried under reduced pressure to afford the desired product as a white powder (0.201 g, 0.31 mmol, 66% yield). X-ray-quality crystals were grown by slow diffusion of Et_2O into a saturated dichloromethane solution. Anal. Found (calcd): C, 44.81 (44.77); H, 5.39 (6.27). ^{31}P NMR ($CDCl_3$): δ_P 3.1 (s, *J*(PtP) = 3559 Hz). ^{1}H NMR ($CDCl_3$): δ_H 7.4−7.5 (m, 3H, Ar *H*), 7.2−7.3 (m, 2H, Ar *H*), 2.5−2.7 (m, 2H), 1.9−2.1 (m, 2H), 1.6−1.9 (m, 4H), 1.3−1.6 (m, 4H). ^{13}C NMR ($CDCl_3$): δ_C 131.7 (t, Ar *C*, *J*(PC) = 5 Hz), 131.1 (m, Ar *C*), 130.9 (s, Ar *C*), 128.6 (t, Ar *C*, *J*(PC) = 5 Hz), 28.1 (s), 27.3 (m), 23.2 (s). FAB mass spectrum: *m*/*z* 650 (M$^+$), 615 (M$^+$ − Cl).

Preparation of *cis*- and *trans*-[$PtCl_2(L^b_5)_2$] ($\mathbf{1b_5}$ and $\mathbf{2b_5}$). To a solution of $\mathbf{L^b_5}$ (0.132 g, 0.92 mmol) in toluene (5 cm^3) was added [$PtCl_2$(cod)] (0.163 g, 0.43 mmol) as a solid. The resulting light yellow solution was stirred for 4 days, after which time a white solid had precipitated. The solid was filtered off, washed with toluene (2 × 2 cm^3), and dried under reduced pressure to give *cis*-[$PtCl_2(\mathbf{L^b_5})_2$] as a fine white powder (0.117 g, 0.21 mmol, 49%). Anal. Found (calcd): C, 35.11 (34.76); H, 6.13 (6.18). ^{31}P NMR (CD_2Cl_2): δ_P 35.7 (s, *J*(PtP) = 3481 Hz). ^{1}H NMR (CD_2Cl_2): δ_H 3.15−2.70 (m, 1H), 2.15−1.20 (br m, 9H), 1.40 (d, 9H, C*H*$_3$,^3J(PH) 14.6 Hz). ^{13}C NMR (CD_2Cl_2): δ_C 34.6−34.1 (m, *C*(CH$_3$)$_3$), 28.6−28.2 (m, *C*H$_3$), 27.2−26.5 (m), 26.9−26.1 (m). CI mass spectrum: *m*/*z* 555 (M$^+$), 520 (M$^+$ − Cl), 484 (M$^+$ − 2Cl). The solvent was removed from the filtrate under reduced pressure to leave *trans*-[$PtCl_2(\mathbf{L^b_5})_2$] as a light yellow solid (0.064 g, 0.12 mmol, 27% yield). Anal. Found (calcd): C, 34.90 (34.66); H, 6.28 (6.18). ^{31}P NMR ($CDCl_3$): δ_P 40.5 (s, *J*(PtP) = 2386 Hz). ^{1}H NMR ($CDCl_3$): δ_H 2.56−2.37 (m, 2H), 1.93−1.65 (m, 6H), 1.23 (t, 9H, C*H*$_3$, *J*(PH) = 7.2 Hz). ^{13}C NMR ($CDCl_3$): δ_C 32.6−32.0 (br m), 28.0−27.4 (br m, *C*H$_3$), 19.6−18.8 (br m). CI mass spectrum: *m*/*z* 554 (M$^+$), 519 (M$^+$ − Cl), 483 (M$^+$ − 2Cl).

Preparation of *cis*- and *trans*-[$PtCl_2(L^b_6)_2$] ($\mathbf{1b_6}$ and $\mathbf{2b_6}$). To a solution of $\mathbf{L^b_6}$ (0.139 g, 0.879 mmol) in toluene (5 cm^3) was added [$PtCl_2$(cod)] (0.164 g, 0.439 mmol) as a solid. The resulting light yellow solution was stirred for 4 days, after which time a white solid had precipitated. The solid was filtered off, washed with toluene (2 × 2 cm^3), and dried under reduced pressure to give *cis*-[$PtCl_2(\mathbf{L^b_6})_2$] as a fine white powder (0.178 g, 0.306 mmol, 82%). X-ray-quality crystals were grown by slow diffusion of Et_2O into a saturated dichloromethane solution. Anal. Found (calcd): C, 37.02 (37.12); H, 6.58 (6.58). ^{31}P NMR (CD_2Cl_2): δ_P 10.6 (s, *J*(PtP) = 3601 Hz). ^{1}H NMR (CD_2Cl_2): δ_H 2.05−1.50 (br m, 10H), 1.34 (d, 9H, C*H*$_3$, ^3J(PH) = 14.6 Hz). ^{13}C NMR (CD_2Cl_2): δ_C 34.5−

33.8 (m), 30.8−30.2 (m), 26.9 (s), 24.9−23.1 (m). CI mass spectrum: *m/z* 583 (M^+), 548 ($M^+ - Cl$), 511 ($M^+ - 2Cl$). The solvent was removed from the filtrate under reduced pressure to leave *trans*-[$PtCl_2$(**L$^b_6$**)$_2$] as a light yellow solid (0.047 g, 0.081 mmol, 18% yield). X-ray-quality crystals were grown by slow diffusion of Et_2O into a saturated CH_2Cl_2 solution. ^{1}H NMR showed the presence of residual CH_2Cl_2 and hence elemental analysis was as follows. Anal. Found (calcd for **2b$_6$**·0.25CH_2Cl_2): C, 36.31 (36.30); H, 5.92 (6.38). ^{31}P NMR ($CDCl_3$): δ_P 16.6 (s, *J*(PtP) = 2433 Hz). ^{1}H NMR ($CDCl_3$): δ_H 3.76−3.69 (m, 2H), 2.76−2.65 (m, 2H), 2.05−1.89 (m, 4H), 1.87−1.78 (m, 2.5H), 1.24 (t, 9H, C*H*$_3$, *J*(PH) = 7 Hz). ^{13}C NMR ($CDCl_3$): δ_C 31.6−31.1 (m, *C*$(CH_3)_3$), 27.6−27.2 (m, *C*H_2), 27.2−26.9 (m, *C*H_3), 23.5−23.1 (m, *C*H_2), 15.6−15.0 (m, *C*H_2). FAB mass spectrum: *m/z* 582 (M^+), 510 ($M^+ - 2Cl$).

Preparation of *cis*- and *trans*-[$PtCl_2$(L$^b_7$)$_2$] (1b$_7$ and 2b$_7$). To a solution of **L$^b_7$** (0.121 g, 0.70 mmol) in toluene (5 cm^3) was added [$PtCl_2$(cod)] (0.125 g, 0.33 mmol) as a solid. The resulting light yellow solution was stirred for 4 days, after which time a white solid had precipitated. The solid was filtered off, washed with toluene (2 × 2 cm^3), and dried under reduced pressure to give *cis*-[$PtCl_2$(**L$^b_7$**)$_2$] as a fine white powder (0.140 g, 0.23 mmol, 69% yield). Anal. Found (calcd): C, 39.29 (39.35); H, 7.05 (6.99). ^{31}P NMR (CD_2Cl_2): δ_P 22.3 (s, *J*(PtP) = 3591 Hz). ^{1}H NMR (CD_2Cl_2): δ_H 3.74−3.58 (m, 1H), 2.43−2.28 (m, 1H), 2.20−1.45 (m, 8H), 1.25 (d, 9H, C*H*$_3$, ^3J(PC) = 14.6 Hz), 1.44−1.2 (m, 2H). ^{13}C NMR (CD_2Cl_2): δ_C 35.5−34.9 (m, *C*$(CH_3)_3$), 30.5 (s), 28.6−28.2 (m, *C*H_3), 26.4−25.8 (m), 24.3−23.8 (m). EI mass spectrum: *m/z* 611 (M^+), 538 ($M^+ - 2Cl$). The solvent was removed from the filtrate under reduced pressure to leave *trans*-[$PtCl_2$(**L$^b_7$**)$_2$] as a light yellow solid (0.034 g, 0.06 mmol, 17% yield). Anal. Found (calcd): C, 39.20 (39.35); H, 7.14 (6.99). ^{31}P NMR (CD_2Cl_2): δ_P 22.9 (s, *J*(PtP) = 2407 Hz). ^{1}H NMR (CD_2Cl_2): δ_H 2.63−2.53 (m, 1H), 2.20−1.05 (m, 11H), 1.24 (t, 9H, C*H*$_3$, *J*(PH) = 6.7 Hz). ^{13}C NMR (CD_2Cl_2): δ_C 32.4 (t, *C*$(CH_3)_3$, *J*(PC) = 15.4 Hz), 28.5 (s, *C*H_2), 27.3 (t, *C*H_3, *J*(PC) = 1.9 Hz), 24.3 (m, *C*H_2), 18.4 (t, *J*(PC) = 14.2 Hz). CI mass spectrum: *m/z* 610 (M^+), 575 ($M^+ - Cl$), 538 ($M^+ - 2Cl$).

Preparation of *cis*- and *trans*-[PtI_2(L$^b_7$)$_2$] (3a$_7$ and 4a$_7$). To a solution of **1a$_7$** (0.050 g, 0.077 mmol) in CH_2Cl_2 (5 cm^3) was added NaI (0.230 g, 1.537 mmol) in acetone (5 cm^3). The resulting yellow solution was stirred for 30 min, and the solvent was removed under reduced pressure. The residue was taken up in dichloromethane, and this solution was washed with water (3 × 10 cm^3) and dried over $MgSO_4$. The solution was filtered and the solvent removed to give a mixture of *cis*- and *trans*-[PtI_2(**L$^b_7$**)$_2$] as a yellow powder (0.061 g, 0.073 mmol, 95% yield). X-ray-quality crystals were grown by slow diffusion of Et_2O into a saturated CH_2Cl_2 solution. ^{31}P NMR ($CDCl_3$): δ_P 2.0 (s, *J*(PtP) = 3400 Hz, 72%), −3.8 (s, *J*(PtP) = 2307 Hz, 28%). ^{1}H NMR ($CDCl_3$): δ_H 7.86−7.78 (m, 2H, Ar *H*), 7.56−7.48 (m, 2H, Ar *H*), 2.43−2.36 (m, 5H, Ar *H*), 7.22−7.28 (m, 1H, Ar *H*), 3.29−3.16 (m, 2H), 2.90−2.77 (m, 2H), 2.55−2.33 (m, 2H), 2.32−2.12 (m, 4H), 1.97−1.60 (m, 12H), 1.58−1.40 (m, 2H). ^{13}C NMR ($CDCl_3$): δ_C 132.1 (m, Ar *C*), 131.9 (m, Ar *C*), 130.6 (s, Ar *C*), 129.9 (s, Ar *C*), 128.5 (m, Ar *C*), 128.2 (m, Ar *C*), 31.6 (s), 31.5 (s), 31.2 (m), 30.4 (m), 29.7 (s), 29.0 (s), 27.7 (s), 27.6 (s), 24.7 (s), 23.9 (s). EI mass spectrum: *m/z* 833 (M^+), 706 ($M^+ - I$), 577 ($M^+ - 2I$).

Preparation of [RhCl(CO)(L$^a_5$)$_2$] (5a$_5$). To a solution of [RhCl(CO)$_2$]$_2$ (0.099 g, 0.255 mmol) in toluene (5 cm^3) was added a solution of **L$^a_5$** (0.186 g, 1.023 mmol) in toluene (2 cm^3). The resulting solution was stirred for 30 min, after which time a sandy brown precipitate had formed. The solvent was removed under reduced pressure to leave the crude product as a brown oil. Recrystallization from a 50/50 dichloromethane/hexane mixture afforded the desired product as yellow crystals suitable for X-ray diffraction. Anal. Found (calcd): C, 51.47 (51.08); H, 5.56 (5.30); Cl, 8.07 (8.77). ^{31}P NMR ($CDCl_3$): δ_P 28.2 (d, *J*(RhP) = 118 Hz). ^{1}H NMR ($CDCl_3$): δ_H 7.5−7.6 (m, 2H, Ar *H*), 7.2−7.3 (m, 3H, Ar *H*), 2.4−2.6 (m, 2H), 2.1−2.3 (m, 2H), 1.7−1.9 (m, 4H). ^{13}C NMR ($CDCl_3$): δ_C 136.6 (d, Ar *C*, *J*(PC) = 18 Hz), 131.1 (t, Ar *C*, *J*(PC) = 6 Hz), 129.3 (s, Ar *C*), 128.4 (t, Ar *C*, *J*(PC) = 5 Hz), 27.5 (t, *C*H_2, *J*(PC) = 14 Hz), 27.0 (s, *C*H_2), CO carbon not seen. IR ν_{CO} (CH_2Cl_2): 1968 cm^{-1}. FAB mass spectrum: *m/z* 494 (M^+), 466 ($M^+ - CO$), 459 ($M^+ - Cl$), 431 ($M^+ - CO - Cl$).

Preparation of [RhCl(CO)(L$^a_6$)$_2$] (5a$_6$). To [RhCl(CO)$_2$]$_2$ (0.073 g, 0.19 mmol) was added a solution of **L$^a_6$** (0.137 g, 0.77 mmol) in hexane (4 cm^3). The solution was stirred for 1 h, during which time the red [RhCl(CO)$_2$]$_2$ was consumed and a fine yellow precipitate formed. The solid was filtered in air, washed with hexane (3 × 1 cm^3), and dried under reduced pressure for 16 h to afford the desired product as a fine light yellow powder (0.168 g, 0.32 mmol, 85% yield). Anal. Found (calcd): C, 53.05 (52.84); H, 5.80 (5.78). ^{31}P NMR ($CDCl_3$): δ_P 6.4 (d, *J*(RhP) = 117 Hz). ^{1}H NMR ($CDCl_3$): δ_H 7.6−7.7 (m, 2H, Ar *H*), 7.3−7.4 (m, 3H, Ar *H*), 2.4−2.5 (m, 2H), 2.1−2.2 (m, 2H), 1.7−2.1 (m, 4H), 1.4−1.7 (m, 2H). ^{13}C NMR ($CDCl_3$): δ_C 187.2 (dt, *C*O, ^1J(RhC) = 75 Hz, ^2J(PC) = 17 Hz), 134 (t, Ar *C*, *J*(PC) = 20 Hz), 131.3 (t, Ar *C*, *J*(PC) = 5 Hz), 129.3 (s, Ar *C*), 128.4 (t, Ar *C*, *J*(PC) = 5 Hz), 27.0 (s, *C*H_2), 24.3 (t, *C*H_2, *J*(PC) = 13 Hz), 22.8 (s, *C*H_2). IR ν_{CO} (CH_2Cl_2): 1960 cm^{-1}. FAB mass spectrum: *m/z* 522 (M^+), 494 ($M^+ - CO$), 487 ($M^+ - Cl$), 179 (P^+).

Preparation of [RhCl(CO)(L$^a_7$)$_2$] (5a$_7$). To [RhCl(CO)$_2$]$_2$ (0.059 g, 0.16 mmol) was added a solution of **L$^a_7$** (0.124 g, 0.65 mmol) in hexane (4 cm^3). The solution was stirred for 1 h, during which time the red [RhCl(CO)$_2$]$_2$ was consumed and a fine yellow precipitate formed. The solid was filtered in air, washed with hexane (3 × 1 cm^3), and dried under reduced pressure for 16 h to afford the desired product as a fine light yellow powder (0.125 g, 0.23 mmol, 71% yield). Anal. Found (calcd): C, 54.76 (54.51); H, 5.88 (6.22). ^{31}P NMR ($CDCl_3$): δ_P 18.1 (d, *J*(RhP) = 118 Hz). ^{1}H NMR ($CDCl_3$): δ_H 7.9−7.8 (m, 2H, Ar *H*), 7.4−7.3 (m, 3H, Ar *H*), 2.7−2.6 (m, 2H), 2.3−2.1 (m, 2H), 2.1−1.8 (m, 6H), 1.7−1.6 (m, 2H). ^{13}C NMR ($CDCl_3$): δ_C 187.9 (dt, *C*O, ^1J(RhC) = 74 Hz, ^2J(PC) = 19 Hz), 136.2 (t, Ar *C*, *J*(PC) = 20 Hz), 132.2 (t, Ar *C*, *J*(PC) = 6 Hz), 129.6 (s, Ar *C*), 128.3 (t, Ar *C*, *J*(PC) = 5 Hz), 28.3 (d, *C*H_2, *J*(PC) = 25 Hz), 28.3 (s, *C*H_2), 24.4 (s, *C*H_2). IR ν_{CO} (CH_2Cl_2): 1962 cm^{-1}. FAB mass spectrum: *m/z* 193 (P^+).

Preparation of [RhCl(CO)(L$^b_5$)$_2$] (5b$_5$). To a solution of **L$^b_5$** (0.172 g, 1.19 mmol) in hexane (10 cm^3) was added [RhCl(CO)$_2$]$_2$ (0.106 g, 0.27 mmol) as a solid. The solution was stirred for 12 h, during which time the red [RhCl(CO)$_2$]$_2$ was consumed and a fine yellow precipitate formed. The solid was filtered in air, washed with hexane (3 × 1 cm^3), and dried under reduced pressure for 16 h to afford the desired product as a fine light yellow powder (0.175 g, 0.39 mmol, 71% yield). X-ray-quality crystals were grown by slow diffusion of hexane into a saturated CH_2Cl_2 solution. Anal. Found (calcd): C, 44.55 (44.90); H, 7.82 (7.54). ^{31}P NMR (CD_2Cl_2): δ_P 49.0 (d, *J*(RhP) = 117 Hz). ^{1}H NMR (CD_2Cl_2): δ_H 2.37−2.26 (m, 2H), 1.95−1.71 (m, 6H), 1.20 (t, 9H, C*H*$_3$, *J*(PH) = 7.1 Hz). ^{13}C NMR (CD_2Cl_2): δ_C 188.6 (dt, *C*O, ^1J(RhC) = 75 Hz, ^2J(PC) = 16 Hz), 32.3 (t, *J*(PC) = 11 Hz), 28.1 (t, *J*(PC) = 3.1 Hz), 28 (s) 23.2 (td, *J*(PC) = 12 Hz, *J*(RhC) = 2 Hz). IR ν_{CO} (CH_2Cl_2): 1955 cm^{-1}. FAB mass spectrum: *m/z* 454 (M^+), 426 ($M^+ - CO$).

Preparation of [RhCl(CO)(L$^b_6$)$_2$] (5b$_6$). To a solution of **L$^b_6$** (0.110 g, 0.70 mmol) in hexane (10 cm^3) was added [RhCl(CO)$_2$]$_2$ (0.065 g, 0.17 mmol) as a solid. The solution was stirred for 12 h, during which time the red [RhCl(CO)$_2$]$_2$ was consumed and a fine yellow precipitate formed. The solid was filtered in air, washed with hexane (3 × 1 cm^3), and dried under reduced pressure for 16 h to afford the desired product as a fine light yellow powder (0.124 g, 0.26 mmol, 77% yield). X-ray-quality crystals were grown by slow diffusion of hexane into a saturated CH_2Cl_2 solution. Anal.

Table 19. Crystallographic Data

	1a$_5$	**1a$_6$**	**1a$_7$**	**1b$_6$**	**2b$_6$**
color, habit	colorless, block	colorless, flat block	colorless, needle	colorless, stalk	yellow, block
size/mm	0.05 × 0.05 × 0.05	0.10 × 0.05 × 0.01	0.3 × 0.06 × 0.05	0.50 × 0.04 × 0.02	0.42 × 0.40 × 0.32
empirical formula	$C_{20}H_{26}Cl_2P_2Pt$	$C_{22}H_{30}Cl_2P_2Pt$	$C_{24}H_{34}Cl_2P_2Pt$	$C_{18}H_{38}Cl_2P_2Pt$	$C_{18}H_{38}Cl_2P_2Pt$
M_r	594.34	622.39	650.44	582.41	582.41
cryst syst	monoclinic	orthorhombic	monoclinic	orthorhombic	monoclinic
space group	*C*2/*c*	*Pna*2$_1$	*C*2/*c*	*Fdd*2	*P*2$_1$/*n*
a/Å	16.511(4)	17.157(2)	20.282(5)	22.400(5)	9.0392(6)
b/Å	8.266(2)	9.1406(10)	10.717(2)	27.229(5)	13.0671(8)
c/Å	16.101(4)	14.2928(13)	11.804(3)	15.047(3)	9.4358(6)
α/deg	90	90	90	90	90
β/deg	106.441(4)	90	109.229(4)	90	97.346(1)
γ/deg	90	90	90	90	90
V/Å^3	2107.5(9)	2241.5(4)	2422.6(10)	9178(3)	1105.37(12)
Z	4	4	4	16	2
μ/mm^{-1}	7.065	6.647	6.154	6.487	6.732
T	173	100	173	173	173
no. of rflns: total/indep (R_{int})	10 703/2411 (0.0358)	24 187/5124 (0.0436)	6136/2769 (0.0409)	14 536/5018 (0.0433)	11 461/2531 (0.0277)
final R1	0.0232	0.0203	0.0329	0.0261	0.0148
largest peak, hole/e Å^{-3}	1.282, −1.112	1.051, −0.467	1.819, −1.528	0.954, −0.706	0.519, −1.177

	4a$_7$	**5a$_5$**	**5b$_5$**	**5b$_6$**	**5b$_7$**
color, habit	yellow plate	yellow prism	yellow block	yellow block	yellow plate
size/mm	0.36 × 0.28 × 0.02	0.30 × 0.10 × 0.1	0.10 × 0.10 × 0.05	0.30 × 0.20 × 0.05	0.20 × 0.20 × 0.05
empirical formula	$C_{24}H_{34}I_2P_2Pt$	$C_{21}H_{26}ClOP_2Rh$	$C_{17}H_{34}ClOP_2Rh$	$C_{19}H_{38}ClOP_2Rh$	$C_{21}H_{42}ClOP_2Rh$
M_r	833.34	494.72	454.74	482.79	510.85
cryst syst	orthorhombic	orthorhombic	triclinic	monoclinic	monoclinic
space group	*Pbca*	*Pbcn*	$P\bar{1}$	*P*2$_1$/*n*	*P*2$_1$/*n*
a/Å	9.1251(10)	9.8155(11)	7.6928(6)	9.0930(14)	8.5201(17)
b/Å	16.8748(18)	17.606(2)	8.0602(7)	13.206(2)	12.871(3)
c/Å	33.956(4)	12.2382(14)	8.9062(7)	9.4945(14)	11.488(2)
α/deg	90	90	89.406(1)	90	90
β/deg	90	90	88.992(1)	97.722(2)	108.41(3)
γ/deg	90	90	68.205(1)	90	90
V/Å^3	5228.7(10)	2115.0(4)	512.68(7)	1129.8(3)	1195.3(5)
Z	8	4	1	2	2
μ/mm^{-1}	7.861	1.093	1.119	1.02	0.968
T	173	173	173	173	100
no. of rflns: total/indep (R_{int})	32 046/5991 (0.0622)	12 764/2439 (0.0640)	4940/2289 (0.0274)	11 705/2582 (0.0304)	3744/2314 (0.0190)
final R1	0.0446	0.0273	0.0316	0.0226	0.0264
largest peak, hole/e Å^{-3}	1.735, −2.872	0.394, −0.518	0.678, −1.039	0.422, −0.280	0.578, −0.518

Found (calcd): C, 47.70 (47.37); H, 8.21 (7.93). ^{31}P NMR (CD_2Cl_2): δ_P 27.8 (d, *J*(RhP) = 118 Hz). ^{1}H NMR (CD_2Cl_2): δ_H 2.36−2.26 (m, 2H), 2.06−1.90 (m, 4H), 1.84−1.74 (m, 1H), 1.63−1.50 (m, 2H), 1.28−1.15 (t, 9H, C*H*$_3$, ^{3}*J*(PH) = 7.1 Hz), 1.28−1.15 (m, 1H). ^{13}C NMR (CD_2Cl_2): δ_C 188.5 (dt, *C*O, *J*(RhC) = 74.6 Hz, *J*(PC) = 16.0 Hz), 31.5 (t, *J*(PC) = 12.3), 27.9 (s), 27.6 (s), 24.2 (s), 20.1 (t, *J*(PC) = 11.1 Hz). IR ν_{CO} (CH_2Cl_2): 1950 cm^{-1}. EI mass spectrum: *m*/*z* 482 (M^+), 454 (M^+ − CO).

Preparation of [RhCl(CO)(L$^b_7$)$_2$] (5b$_7$). To a solution of **L$^b_7$** (0.149 g, 0.87 mmol) in hexane (10 cm^3) was added $[RhCl(CO)_2]_2$ (0.084 g, 0.22 mmol) as a solid. The solution was stirred for 12 h, during which time the red $[RhCl(CO)_2]_2$ was consumed and a fine yellow precipitate formed. The solid was filtered in air, washed with hexane (3 × 1 cm^3), and dried under reduced pressure for 16 h to afford the desired product as a fine light yellow powder (0.138 g, 0.27 mmol, 63% yield). X-ray-quality crystals were grown by slow diffusion of hexane into a saturated CH_2Cl_2 solution. Anal. Found (calcd): C, 49.16 (49.37); H, 8.24 (8.29). ^{31}P NMR (CD_2Cl_2): δ_P 34.8 (d, *J*(RhP) = 118 Hz). ^{1}H NMR (CD_2Cl_2): δ_H 2.38−2.29 (m, 2H), 2.06−1.64 (m, 8H), 1.58−1.46 (m, 2H), 1.22 (t, C*H*$_3$, 9H, *J*(PC) = 6.6 Hz). ^{13}C NMR (CD_2Cl_2): δ_C 188.3 (dt, *C*O, *J*(RhC) = 74.6 Hz, *J*(PC) = 16.1 Hz), 32.1 (t, *C*(CH$_3$), *J*(PC) = 12.7 Hz), 28.3 (s), 27.8 (t, *J*(PC) = 2.7 Hz), 25.0 (s, *C*H$_3$), 22.5 (dt, *C*H$_2$P, *J*(RhC) = 1.5 Hz, *J*(PC) = 10.8 Hz). IR ν_{CO} (CH_2Cl_2): 1951 cm^{-1}. EI mass spectrum: *m*/*z* 510 (M^+).

Kinetic Experiments. Reaction monitoring for kinetic experiments was achieved using a Perkin-Elmer GX FTIR spectrometer controlled by Spectrum TimeBase software. Pseudo-first-order conditions were employed, with at least a 10-fold excess of MeI, relative to the Rh complex. A solution containing the required concentration of MeI in CH_2Cl_2 was prepared in a 5 cm^3 graduated flask. A portion of this solution was used to record a background spectrum. Another portion (typically 500 μL) was added to the solid Rh complex in a sample vial to give a reaction solution containing typically 5−10 mM [Rh]. A portion of the reaction solution was quickly transferred to the IR cell, and data collection was started. The IR cell (0.5 mm path length, CaF_2 windows) was maintained at constant temperature by a thermostated jacket. Spectra (2200−1600 cm^{-1}) were scanned and saved at regular time intervals under computer control. Absorbance vs time data for the appropriate *ν*(CO) frequencies were extracted and analyzed off-line using Kaleidagraph curve-fitting software. For each experiment, the decay of the reactant *ν*(CO) band was fitted to an exponential curve, with correlation coefficient ≥0.999, to give the pseudo-first-order rate constant. Each kinetic run was repeated at least twice to check reproducibility, the k_{obs} data given being averaged values with component measurements deviating from each other by ≤5%.

Hydroformylation Catalysis. The phosphine (0.112 mmol) and $[Rh(CO)_2(acac)]$ (3.0 mg, 0.012 mmol) were dissolved in toluene (10 cm^3) under nitrogen in a Schlenk tube. The resulting solution was transferred by cannula to a 100 mL autoclave, which had been flushed three times with 3 bar of CO/H_2 (1/1). The autoclave was then pressurized with 2 bar of CO/H_2 (1/1) at room temperature. The reaction mixture was then stirred vigorously with a sparging stirrer and heated to 90 °C over a period of 30 min. After this preactivation of the catalyst, 1-octene (10 g) was introduced into

the autoclave via a lock by means of CO/H_2 pressure. The pressure was then immediately raised to 10 bar and maintained at this pressure throughout the catalysis by introduction of further CO/H_2 (1/1) via a pressure regulator. After the reactions were run for 4 h, the autoclave was cooled, vented, and emptied. Analysis of the reaction products was carried out by GC.

X-ray Crystal Structure Analyses. X-ray diffraction experiments on **1a$_5$**, **1a$_7$**, **1b$_6$**, **2b$_6$**, **4a$_7$**, **5a$_5$**, **5b$_5$**, and **5b$_6$** were carried out at 173 K on a Bruker SMART diffractometer, and experiments on **1a$_6$** and **5b$_7$** were carried out at 100 K on a Bruker SMART APEX diffractometer, both using Mo Kα X-radiation ($\lambda = 0.710\ 73$ Å) and a CCD area detector, from a single crystal coated in paraffin oil mounted on a glass fiber. Intensities were integrated[32] from several series of exposures, each exposure covering 0.3° in ω. Absorption corrections were based on equivalent reflections using SADABS V2.10,[33] and structures were refined against all F_o^2 data with hydrogen atoms riding in calculated positions using SHELXTL.[34] Crystal and refinement data are given in Table 19. For **1b$_6$**, the position of one of the *tert*-butyl groups is disordered and has been modeled as sitting over two positions, with occupancies of 0.33 and 0.67. In compounds **5b$_{5-7}$**, each complex contains a crystallographic center of inversion, meaning that the carbonyl and chloride ligands are disordered over two sites, each with occupancies of 0.5. The chloride and carbonyl ligands are not disordered in **5a$_5$**.

Acknowledgment. We thank Dr. Paul Elliott (University of Sheffield) for assistance with the kinetic experiments, Qiang Miao (BASF) for assistance with the Experimental Section, BASF and EPSRC for financial support, The Leverhulme Trust for a Fellowship (to P.G.P.), and Johnson-Matthey for the loan of precious metal compounds.

Supporting Information Available: CIF files giving crystallographic data for **1a$_{5-7}$**, **4a$_7$**, **1b$_6$**, **2b$_6$**, **5a$_5$**, and **5b$_{5-7}$** and tables and figures giving kinetic data, including plots of k_{obs} against [MeI] and Eyring plots. This material is available free of charge via the Internet at http://pubs.acs.org.

OM060912V

(32) SAINT Integration Software; Siemens Analytical X-ray Instruments Inc., Madison, WI, 1994.

(33) Sheldrick, G. M. SADABS V2.10; University of Göttingen, Göttingen, Germany, 2003.

(34) SHELXTL Program System, Version 5.1; Bruker Analytical X-ray Instruments Inc., Madison, WI, 1998.